Calhoun: The NPS Institutional Archive

DSpace Repository

Theses and Dissertations 1. Thesis and Dissertation Collection, all items

1983

Baroclinic Rossby wave signature in a general circulation ocean model.

Rutsch, Arno H.

Monterey, California. Naval Postgraduate School

http://hdl.handle.net/10945/19655

Downloaded from NPS Archive: Calhoun

Calhoun is the Naval Postgraduate School's public access digital repository for research materials and institutional publications created by the NPS community. Calhoun is named for Professor of Mathematics Guy K. Calhoun, NPS's first appointed -- and published -- scholarly author.

Dudley Knox Library / Naval Postgraduate School
411 Dyer Road / 1 University Circle
Monterey, California USA 93943

http://www.nps.edu/library

Dudley Knox Library, NPS
Monterey, CA 93943

NAVAL POSTGRADUATE SCHOOL

Monterey, California

THESIS

BAROCLINIC ROSSBY WAVE SIGNATURE IN A GENERAL CIRCULATION OCEAN MODEL

by

Arno H. Rutsch

June 1983

Thesis Advisor: R. L. Haney

Approved for public release; distribution unlimited.

T208952

REPORT DOCUMENTATION PAGE		READ INSTRUCTIONS BEFORE COMPLETING FORM
1. REPORT NUMBER	2. GOVT ACCESSION NO.	3. RECIPIENT'S CATALOG NUMBER
4. TITLE (and Subtitle) Baroclinic Rossby Wave Signature in a General Circulation Ocean Model		5. TYPE OF REPORT & PERIOD COVERED Master's Thesis June 1983
		6. PERFORMING ORG. REPORT NUMBER
7. AUTHOR(s) Arno H. Rutsch		8. CONTRACT OR GRANT NUMBER(s)
9. PERFORMING ORGANIZATION NAME AND ADDRESS Naval Postgraduate School Monterey, California 93940		10. PROGRAM ELEMENT, PROJECT, TASK AREA & WORK UNIT NUMBERS
11. CONTROLLING OFFICE NAME AND ADDRESS Naval Postgraduate School Monterey, California 93940		12. REPORT DATE June 1983
		13. NUMBER OF PAGES 70
14. MONITORING AGENCY NAME & ADDRESS(if different from Controlling Office)		15. SECURITY CLASS. (of this report)
		15a. DECLASSIFICATION/DOWNGRADING SCHEDULE

16. DISTRIBUTION STATEMENT (of this Report)

Approved for public release; distribution unlimited.

17. DISTRIBUTION STATEMENT (of the abstract entered in Block 20, if different from Report)

18. SUPPLEMENTARY NOTES

19. KEY WORDS (Continue on reverse side if necessary and identify by block number)

Baroclinic Rossby Waves
General Circulation Ocean Model Evaluation
Large-Scale Ocean Dynamics
North Pacific Ocean Dynamics
Model Simulated Ocean Temperature Variability

20. ABSTRACT (Continue on reverse side if necessary and identify by block number)

Monthly mean values of temperature output for a ten-year period (1969-78) from a three-dimensional primitive equation ocean model are used to compute isotherm displacements at eight selected grid points in the North Pacific Ocean. The ocean model input parameters are climatological radiation, clouds, surface air temperature, surface humidity and six-hourly synoptic winds taken from Fleet Numerical Oceanography

Center analyses. The first five baroclinic modes are computed from the mean temperature profiles at the eight selected model grid points and these modes are then fit in the time domain to the isotherm displacements.

The fit shows evidence of baroclinic free Rossby waves in the time domain at the selected grid points south of 40N and indicates the predominance of the first baroclinic mode. At the selected grid points north of 40N, the results are inconclusive. This is due to the longer periods required at the northern latitudes, the neglect of salinity, and masking by a strong seasonal signal caused by surface heating and cooling at higher latitudes.

Approved for public release; distribution unlimited

Baroclinic Rossby Wave Signature in a General Circulation Ocean Model

by

Arno H Rutsch
Lieutenant, United States Navy
B.S. University of Michigan, 1974

Submitted in partial fulfillment of the
requirements for the degree of

MASTER OF SCIENCE IN METEOROLOGY AND OCEANOGRAPHY

from the

NAVAL POSTGRADUATE SCHOOL
June 1983

Dudley Knox Library, NPS
Monterey, CA 93943

ABSTRACT

Monthly mean values of temperature output for a ten-year period (1969-78) from a three-dimensional primitive equation ocean model are used to compute isotherm displacements at eight selected grid points in the North Pacific Ocean. The ocean model input parameters are climatological radiation, clouds, surface air temperature, surface humidity and six-hourly synoptic winds taken from Fleet Numerical Oceanography Center analyses. The first five baroclinic modes are computed from the mean temperature profiles at the eight selected model grid points and these modes are then fit in the time domain to the isotherm displacements.

The fit shows evidence of baroclinic free Rossby waves in the time domain at the selected grid points south of 40N and indicates the predominance of the first baroclinic mode. At the selected grid points north of 40N, the results are inconclusive. This is due to the longer periods required at the northern latitudes, the neglect of salinity, and masking by a strong seasonal signal caused by surface heating and cooling at higher latitudes.

TABLE OF CONTENTS

I. INTRODUCTION 10

II. MODEL DESCRIPTION AND ANALYSIS PROCEDURE 12

  A. MODEL DESCRIPTION 12

  B. ANALYSIS PROCEDURE 14

    1. Governing Equations for Baroclinic Rossby Waves 14

    2. Determination of N^2 and The Isotherm Displacement Field 19

    3. The Solution of The Vertical Problem . . . 28

III. RESULTS 46

IV. CONCLUSIONS AND RECOMMENDATIONS 65

LIST OF REFERENCES 68

INITIAL DISTRIBUTION LIST 69

LIST OF FIGURES

Figure 1. Horizontal Domain of Ocean Model 13

Figure 2. Profiles of $(\overline{N^2})^{1/2}$ at Latitudes 18.3N and 24.4N 23

Figure 3. Profiles of $(\overline{N^2})^{1/2}$ at Latitudes 30.5N and 36.6N 24

Figure 4. Profiles of $(\overline{N^2})^{1/2}$ at Latitudes 42.7N and 48.8N 25

Figure 5. Profile of $(\overline{N^2})^{1/2}$ at Latitude 54.8N 26

Figure 6. Isotherm Displacement at 30.5N 139.1W for Levels 1 to 6 29

Figure 7. Isotherm Displacement at 30.5N 139.1W for Levels 7 to 12 30

Figure 8. Isotherm Displacement at 30.5N 139.1W for Levels 13 to 19 31

Figure 9. Eigencurves and Eigenvalues for Latitude 30.5N 34

Figure 10. Normalized Eigenfunctions at 18.3N 37

Figure 11. Normalized Eigenfunctions at 24.4N 38

Figure 12. Normalized Eigenfunctions at 30.5N 39

Figure 13. Normalized Eigenfunctions at 36.6N 40

Figure 14. Normalized Eigenfunctions at 42.7N 41

Figure 15. Normalized Eigenfunctions at 48.8N 42

Figure 16. Normalized Eigenfunctions at 54.8N 43

Figure 17. $A_n(t)$ and DEV(t) at 18.3N 155.9W 47

Figure 18. $A_n(t)$ and DEV(t) at 24.4N 155.9W 48

Figure 19. $A_n(t)$ and DEV(t) at 30.5N 155.9W 49

Figure 20. $A_n(t)$ and DEV(t) at 36.6N 155.9W 50

Figure 21. $A_n(t)$ and DEV(t) at 42.7N 155.9W 51

Figure 22. $A_n(t)$ and DEV(t) at 48.8N 155.9W 52

Figure 23. $A_n(t)$ and DEV(t) at 54.8N 155.9W 53

Figure 24. $A_n(t)$ and DEV(t) at 30.5N 139.1W 54

Figure 25. $A_n(t)$, and DEV(t) for weather station November 56

Figure 26. Cutoff Period versus Latitude 58

Figure 27. Locus of Wave Number Vectors for Mode 1 at 18.3N 61

Figure 28. Locus of Wave Number Vectors for Mode 1 at 36.6N 62

LIST OF TABLES

TABLE I. Reciprocal Eigenvalues(m/sec) for Modes 1 to 5 35

TABLE II. Mean Deviation (%) at Selected Grid Points . 57

ACKNOWLEDGEMENT

The author expresses his sincere gratitude to Dr. Robert Haney for not only his contributions as thesis advisor but also for providing the model simulated temperature data, for helping define the study and for providing recommendations, both editorial and theoretical. Without his help the development of this thesis would have been impossible.

The author additionally expresses his gratitude to Dr. Andrew Willmott for providing not only editorial recommendations but also guidance pertaining to the mathematical and theoretical development of the baroclinic Rossby wave equation. Appreciation is also expressed to Dr. Rudolf Preisendorfer for his guidance regarding the numerical solution of the governing equation for baroclinic Rossby waves. Finally, the author expresses his deepest gratitude to his wife, Sheryl, and son, Michael, for their support and patience.

The author utilized the computing facilities of the W. R. Church Computer Center at the Naval Postgraduate School while conducting this study.

I. INTRODUCTION

Oceanic general circulation models have been under development for the past decade and a half. Evaluation of these newly developed models was initially hindered by a lack of adequate observational data from ocean regions. However, over the past eight years high quality oceanic data and data analysis studies from portions of the ocean have been made available to the large-scale ocean modeller. Of particular importance and interest in this study has been the analyses of temperature data resulting from the "North Pacific Experiment" (NORPAX) begun during the last decade.

Based upon an analysis of TRANSPAC data (a sub-program of NORPAX confined to a region 30-50N and 170E - 150W), Kang and Magaard (1980) determined that annual temperature fluctuations in the area 30-40N, 160E - 130W consisted of first mode Rossby waves with random phase traveling northwest with a wavelength of 300 km. For other latitudes of the North Pacific Ocean, Price and Magaard (1980) determined that first mode baroclinic Rossby waves with dominant period of seven to ten years existed in the region 40-50N. It was also determined that Rossby waves of annual period did not play a role in the latitude belt 40-50N in the North Pacific

Ocean. Magaard (1983), in a paper discussing baroclinic Rossby wave energetics, summarizes these earlier studies by stating that first mode baroclinic Rossby waves dominate the internal temperature fluctuations in the region 20-30N in the North Pacific Ocean for a whole range of periods between five months and ten years. Between 30-40N only annual or near-annual first mode baroclinic Rossby waves are evident. It is the results of these studies that have motivated this investigation, which is essentually an evaluation of whether a general circulation ocean model, driven by observed synoptic winds, can simulate the above characteristics of the North Pacific Ocean Rossby wave field. Following a procedure outlined by Emery and Magaard (1976), this study examines the possible existence of baroclinic Rossby waves inferred from temperature fields produced by the ocean model.

II. MODEL DESCRIPTION AND ANALYSIS PROCEDURE

A. MODEL DESCRIPTION

The model used in this study is a three-dimensional primitive equation model developed at the Naval Postgraduate School and described by Haney (1980). A flat bottom and rigid lid are prescribed. The model is driven by seasonally varying (monthly climatology) solar radiation, clouds, surface air temperature, and surface relative humidity. The surface winds utilized are taken from six-hourly synoptic analyses, 1969-1978, made at the Fleet Numerical Oceanography Center, Monterey, California. Salinity is neglected. The model domain shown in Figure 1 is a rectangular basin extending from the Equator to 65N and from 145E - 125W. The horizontal grid spacing is approximately two degrees in latitude and three degrees in longitude. The model is 4000 m deep with 20 irregularly spaced levels, 14 of which are above 1000 m. The boundary conditions prescribed at the bottom and sides are those of an enclosed thermally insulated basin.

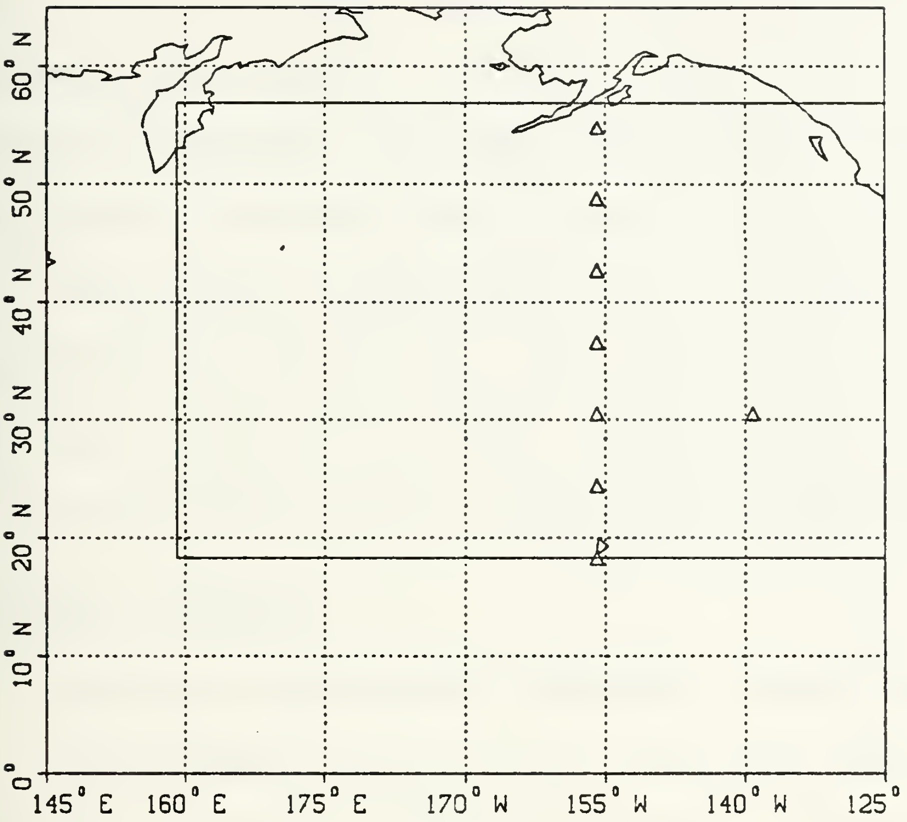

Horizontal domain of temperature field used for analysis is shown by enclosed region. Triangles mark grid points selected for Rossby wave analysis.

Figure 1. Horizontal Domain of Ocean Model

The model also includes a dynamic adjustment mechanism as described by Adamec, et. al. (1981). Essentially, the mechanism assures that if the local gradient Richardson number, Ri, falls below a critical value (0.25) then the temperature and the velocity components at the two adjacent levels are mixed vertically so that heat and momentum are

conserved, the mixing ratios for heat and momentum are equal, and after mixing Ri equals the critical value.

The model was run for a 30-year period, with the first two decades considered as a "spin-up" period and the third decade, 1969-78, considered as a simulation of actual conditions. The purpose of this thesis is to analyze the temperature variability simulated by the model during this last decade. The goal is to see if the variability is consistent with the dispersion relation for baroclinic Rossby waves.

B. ANALYSIS PROCEDURE

1. Governing Equations for Baroclinic Rossby Waves

The governing equations for baroclinic Rossby waves are derived from the frictionless momentum equations, the hydrostatic balance, and the continuity equation for an incompressible fluid in the following form:

$$u_t + (V\cdot\nabla)u - fv + \frac{1}{\rho} p_x = 0 \ , \tag{1a}$$

$$v_t + (V\cdot\nabla)v + fu + \frac{1}{\rho} p_y = 0 \ , \tag{1b}$$

$$\nabla\cdot V = 0 \ , \tag{1c}$$

$$p_z + \rho g = 0 \ , \tag{1d}$$

$$\rho_t + (V\cdot\nabla)\rho = 0 \ , \tag{1e}$$

where V is the velocity vector, u, v and w are the velocity components in the eastward (x), northward (y), and upward (z) direction, respectively, ρ is the density, p is the pressure, g is the acceleration due to gravity, f is the Coriolis parameter, t is time and $\nabla = (\frac{\partial}{\partial x}, \frac{\partial}{\partial y}, \frac{\partial}{\partial z})$. The subscripts denote partial differentiation with respect to the subscripted variable.

The vorticity equation is formed using equations (1a) and (1b). Subsequent application of the quasi-geostrophic approximation and linearization leads to the following form of the vorticity equation:

$$(p'_{xx} + p'_{yy})_t + \beta p'_x - \rho_o f^2 w'_z = 0 \; , \qquad (2)$$

where p' and w' are the perturbation pressure and vertical velocity component, $\beta = df/dy$, ρ_o is a constant reference density, and the other variables are as defined before. Additional assumptions used in the above linearization process are that the lateral shear of the basic flow is neglected and the basic state horizontal velocity is at rest (i.e., $\bar{u} = \bar{v} = 0$). From this assumption, equation (1c) and the boundary condition that w = 0 at z = 0 (sea surface) it

follows that $\bar{w} = 0$. Equation (2) contains two unknown variables, p' and w', therefore, an additional equation is required.

Substituting from (1d) into (1e) after multiplying by $-g/\rho_o$ and subsequent linearization yields the second equation,

$$p'_{zt} + \rho_o N^2 w' = 0 \tag{3a}$$

or

$$w' = - \left(\frac{1}{N^2 \rho_o}\right) p'_{zt} \; , \tag{3b}$$

where $N^2 = -(g/\rho_o)\bar{\rho}_z$ is the Brunt-Väisälä frequency squared, assumed to be a function of z only. Eliminating w' in (2) using (3b) yields,

$$(p'_{xx} + p'_{yy})_t + \beta p'_x + f^2 \left[\frac{1}{N^2} p'_{zt}\right]_z = 0 \; . \tag{4}$$

Using the separation of variables technique the perturbation pressure is written,

$$p'(x,y,z,t) = P_n(z) \, \hat{p}_n(x,y,t) \; , \tag{5}$$

where n is the mode number. Substituting (5) into equations (4) and (3b) gives,

$$-\frac{1}{P_n}\frac{d}{dz}\left[\frac{1}{N^2}\frac{dP_n}{dz}\right] = \frac{\nabla^2(\hat{p}_n)_t + \beta(\hat{p}_n)_x}{f^2(\hat{p}_n)_t} = \lambda_n{}^2 , \tag{6}$$

and

$$\frac{1}{N^2}\frac{dP_n}{dz} = -\frac{\rho_o\, w'}{(\hat{p}_n)_t} . \tag{7}$$

where $\nabla^2 = (\frac{\partial^2}{\partial x^2}, \frac{\partial^2}{\partial y^2})$, and λ_n^2 is a separation constant with dimensions of inverse velocity. Differentiating equation (6) with respect to z yields,

$$\frac{d^2}{dz^2}\left[\frac{1}{N^2}\frac{dP_n}{dz}\right] + \lambda_n{}^2\frac{dP_n}{dz} = 0 . \tag{8}$$

Substituting from equation (7) into equation (8) yields the governing equation or vertical equation,

$$\frac{d^2w_n'}{dz^2} + \lambda_n{}^2 N^2(z)w_n' = 0 \tag{9a}$$

subject to boundary conditions,

$$\begin{aligned} w' &= 0 \quad \text{at } z = 0 \text{ (Sea Surface)} \\ w' &= 0 \quad \text{at } z = -H \text{ (Sea Bottom)} \end{aligned} \tag{9b}$$

Equation (6) written in the form,

$$\nabla^2(\hat{p}_n)_t - \lambda_n^2 f^2(\hat{p}_n)_t + \beta(\hat{p}_n)_x = 0 \qquad (10a)$$

represents the Rossby wave equation for which solutions of the form

$$\hat{p}_n = \mathrm{EXP}[i(kx + \ell y - \sigma t)] \ , \qquad (10b)$$

are sought where k and ℓ are wavenumbers in the x and y direction, respectively and σ is the frequency. Substituting from (10b) into (10a) yields a form of the dispersion relationship for baroclinic Rossby waves, viz.,

$$\lambda_n{}^2 = \frac{-\beta k - \sigma(k^2 + \ell^2)}{\sigma f^2} \ . \qquad (11)$$

Equation set (9) forms a Sturm-Liouville eigenvalue problem for the vertical motion, where λ_n are the eigenvalues and w_n' the corresponding eigenfunctions. A solution is sought for a finite number of modes, m. These modes correspond to the first m baroclinic Rossby wave modes.

If N(z) were independent of depth at a fixed location and time, the solution for w_n' could be readily

determined analytically as trigonometric functions of $(n\pi z)/H$ (see for example Pedlosky (1979, pp. 356-360)), provided

$$\lambda_n = \frac{n\pi}{NH} ; \quad n = 1,2,3,\ldots \quad (12)$$

In certain instances an analytical solution to equation set (9) can be found provided $N^2(z)$ is, or approximates, a well defined function (see for example Willmott and Mysak (1980) who solve the vertical problem with $N^2(z)$ as an exponential function of z). Realistic distributions of N^2 are dependent upon depth and generally not well defined functions of z, therefore the solution of equation set (9) is obtained numerically.

2. Determination of N^2 and The Isotherm Displacement Field

The Brunt-Väisälä frequency squared is, as defined earlier, equal to $-(g/\rho_o)\bar{\rho}_z$. Since the model neglects salinity, the simple state relation,

$$\bar{\rho} = \rho_o[1 - \alpha(\bar{T} - T_o)] , \quad (13)$$

is used to convert the Brunt-Väisälä frequency squared from a function of the vertical mean density gradient into a

function of the vertical mean temperature gradient, where T_0 is a constant reference temperature and α is the coefficient of thermal expansion. Differentiating equation (13) with respect to z and substituting into the definition of N^2 gives,

$$N^2 = \alpha g \, \bar{T}_z \; . \qquad (14)$$

Equation (14) is used to calculate N^2 from the mean monthly temperature fields output by the ocean model for the last ten years, 1969-78, of the model run. Only the temperature field in the region 18.3 - 56.9N and 159.1E - 125W shown as the enclosed box in Figure 1 is used in the calculation of N^2. After completion of the numerical differentiation (right side of equation (14)), a ten-year time mean, $\bar{N}^2$, at each grid point and at 19 vertical levels (mid-levels of the 20 model levels) is calculated. Finally $\bar{N}^2$ is averaged over 28 east-west grid points, giving a $\bar{N}^2$ versus depth profile for each latitude (20 north-south grid points). Justification for the east-west averaging is based upon little variability of $\bar{N}^2$ with longitude over the region at a particular vertical level. The variability of $\bar{N}^2$ with latitude, on

the other hand, is such that north-south averaging is not justified. Price and Magaard (1980) also found that mean N^2 profiles varied much more with latitude than with longitude, and thus the numerical model data are consistent with the corresponding data taken from the North Pacific Ocean. Profiles of $(\bar{N}^2)^{1/2}$, averaged over longitude, are shown in Figures 2 to 5 for the latitudes of the grid points selected in this investigation (triangular symbols on Figure 1). The solid curves on each figure are drawn to the values of $(\bar{N}^2)^{1/2}$ at 19 vertical levels determined by equation (14). The dashed curves are drawn to values of $(\bar{N}^2)^{1/2}$ calculated at every five meters from $z = 0$ to $z = -4000$ m using interpolation. The interpolation is done numerically by means of Aitken's scheme of Lagrange interpolation described by Hildebrand (1956, pp. 49-50) using the values of $(\bar{N}^2)^{1/2}$ at the 19 vertical levels and an assigned value of $(\bar{N}^2)^{1/2}$ at -4000 m as tabular input. At latitude 48.8N and 54.8N the assigned bottom value for $(\bar{N}^2)^{1/2}$ was given the identical value calculated at level 19 (2830 m). At the other selected latitudes the assigned bottom value was determined by linear extrapolation using the levels below 1000 m (levels 15 to 19).

The profiles show a pronounced variability with latitude. Below approximately 900 m, $(\bar{N}^2)^{1/2}$ is small (less than 0.001 1/sec) and nearly constant (model simulated isothermal condition in the deep ocean). At latitudes north of 47N this constancy is evident at depths below 150 m. The maximum value of $(\bar{N}^2)^{1/2}$ (maximum vertical temperature gradient) occurs at level 2 (16.5 m) at latitudes south of 22N and between latitude 40N and 50N. At the other latitudes the maximum occurs near the surface (5 m). A secondary maximum occurs between latitudes 30N and 45N at a depth between 200 m and 400 m (inferred location of the mean thermocline).

The second field to be computed using the model simulated mean monthly temperature fields is the isotherm displacement. The isotherm displacement, D(z,t), is the displacement of a monthly mean isotherm from its long-term average level. It is defined mathematically as $-T'/(\bar{T})_z$ where T' is the temperature fluctuation, $T' = T - \bar{T}$. $\bar{T}$ and $(\bar{T})_z$ are the long-term (ten-year) averaged temperature and vertical temperature gradient, respectively. In the numerical calculation of D(z,t) the assumption is made that the temperature field is linear in z between model levels. The isotherm displacement versus time curves at 19 vertical

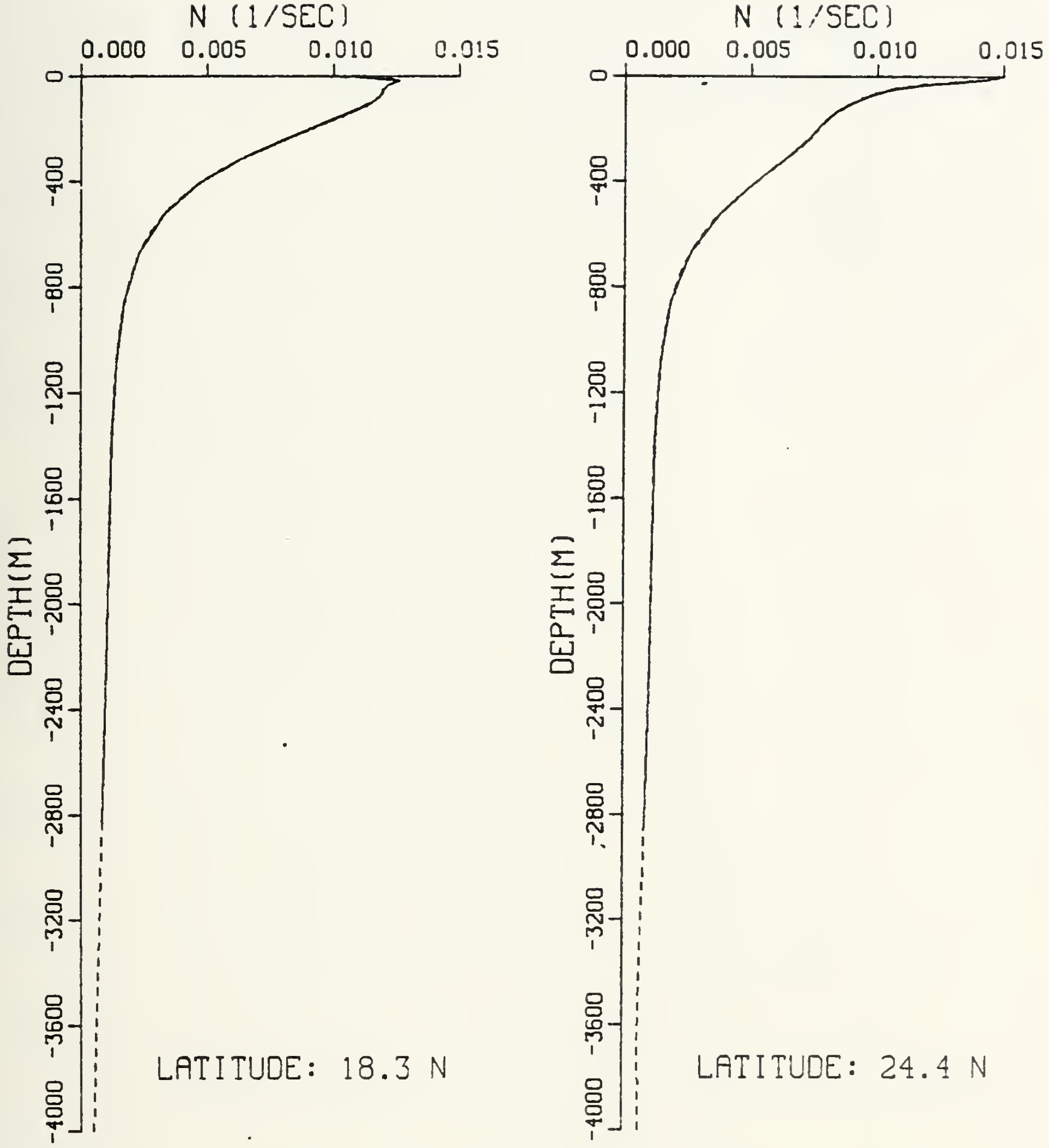

Figure 2. Profiles of $(\bar{N}^2)^{1/2}$ at Latitudes 18.3N and 24.4N

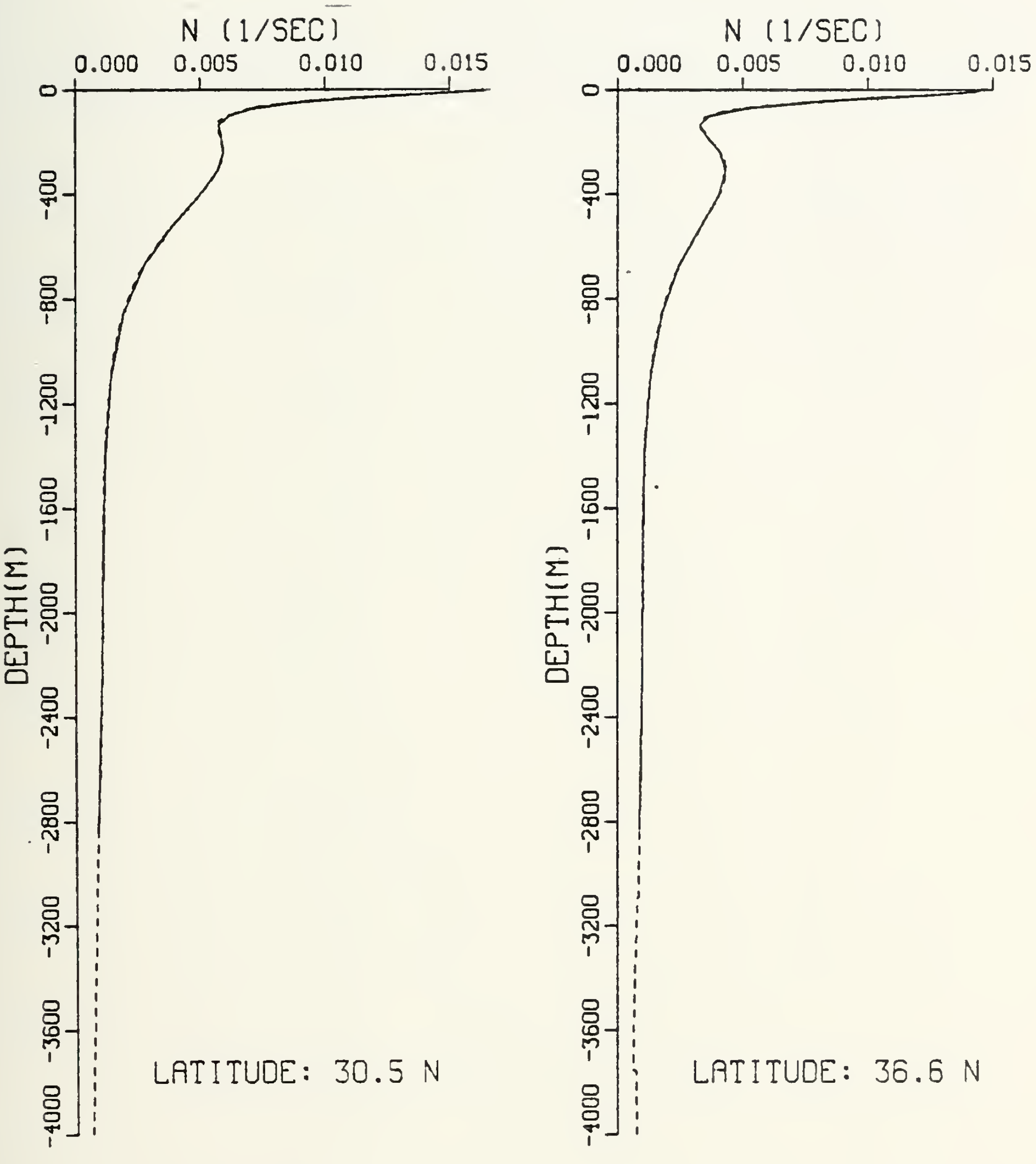

Figure 3. Profiles of $(\bar{N}^2)^{1/2}$ at Latitudes 30.5N and 36.6N

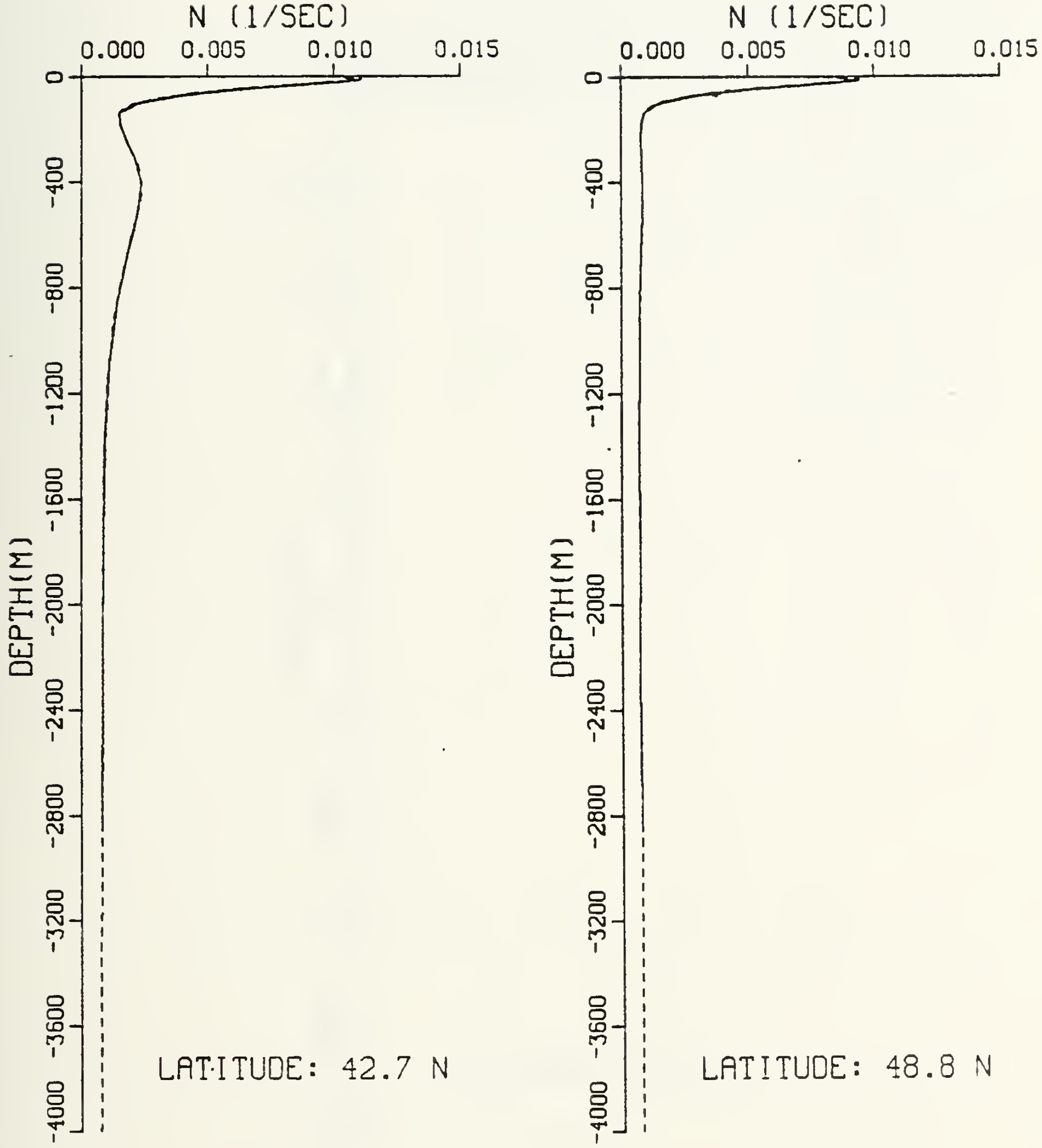

Figure 4. Profiles of $(\overline{N^2})^{1/2}$ at Latitudes 42.7N and 48.8N

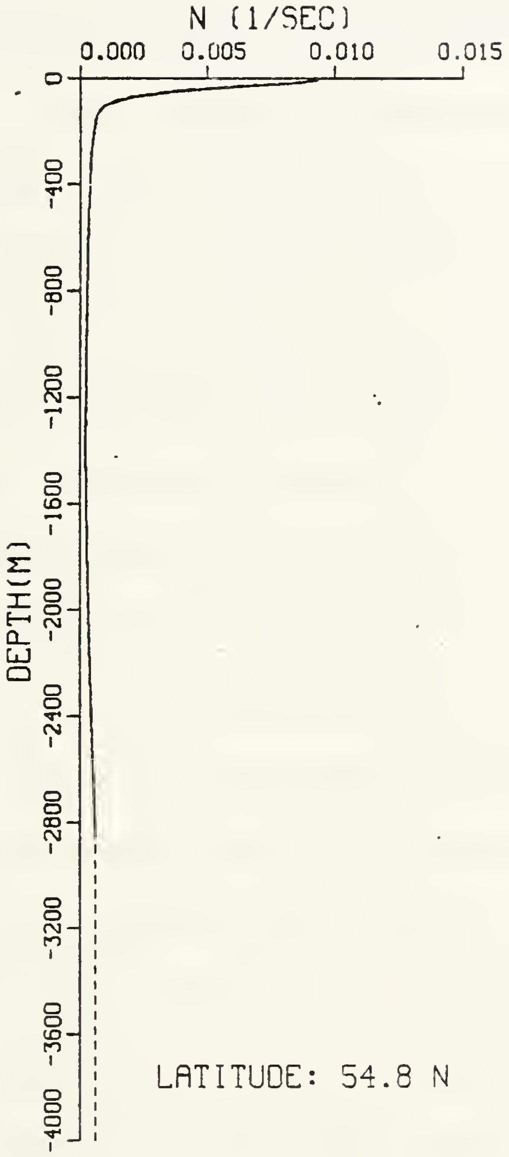

Figure 5. Profile of $(\bar{N}^2)^{1/2}$ at Latitude 54.8N

levels from the ten-year model simulation are shown in Figures 6, 7, and 8 for the grid point at 30.5N 139.1W.

By virtue of its definition, D(z,t) positive, in general, implies a temperature colder than the long-term mean. D(z,t) negative implies a temperature warmer than the long-term mean. The isotherm displacement curves, as depicted in Figures 6 to 8, reveal a pronounced seasonal signal (annual period) at levels above 71.5 m. At 100 m (level 6) and below the seasonal signal becomes less well defined and losses definition with depth. The seasonal signal at the upper levels is primarily the model simulated mean monthly temperature fields response to the seasonally varying solar radiation provided as model input. Below 100 m (Figures 7 and 8) a low frequency (long period) signal is evident. The isotherm displacement curves at the other selected grid points (not shown), in general, show similar characteristics of an upper level annual cycle and low frequency signal at lower levels. The significant features, proceeding from south to north at longitude 155.9W, are that, 1) the depth at which the seasonal signal remains distinguishable increases reaching 1760 m (level 17) at 54.8N, 2) the amplitude of the isotherm displacement at

mid-levels increases from a maximum of approximately 50 m at 18.3N to 5000 m at 54.8N. This increase in amplitude is a result of the near isothermal conditions evident below 150 m at the northern latitudes (i.e. $(\bar{T})_z$ is small thereby increasing the value of D(z,t)).

3. The Solution of The Vertical Problem

Equation set (9) is solved numerically using an Interactive Ordinary Differential Equation (IODE) solver which uses a fourth-order Runge-Kutta integration technique. The eigenvalues, λ_n, are found by means of the "c-root method" described by Preisendorfer and Gonzalez (1973). In applying the "c-root method" equation (9a) is separated into two first-order differential equations,

$$\frac{dw_n'}{dz} = \phi \qquad (15a)$$

$$\frac{d\phi}{dz} = -\lambda_n^2 \bar{N}^2(z) w_n' \; . \qquad (15b)$$

A trial value is choosen for λ, and equations (15a) and (15b) are integrated using IODE starting at the sea bottom, z = -H (4000 m), with boundary values of $w_n' = 0$ and $\phi = 1$. As the integration proceeds the zeros of the function

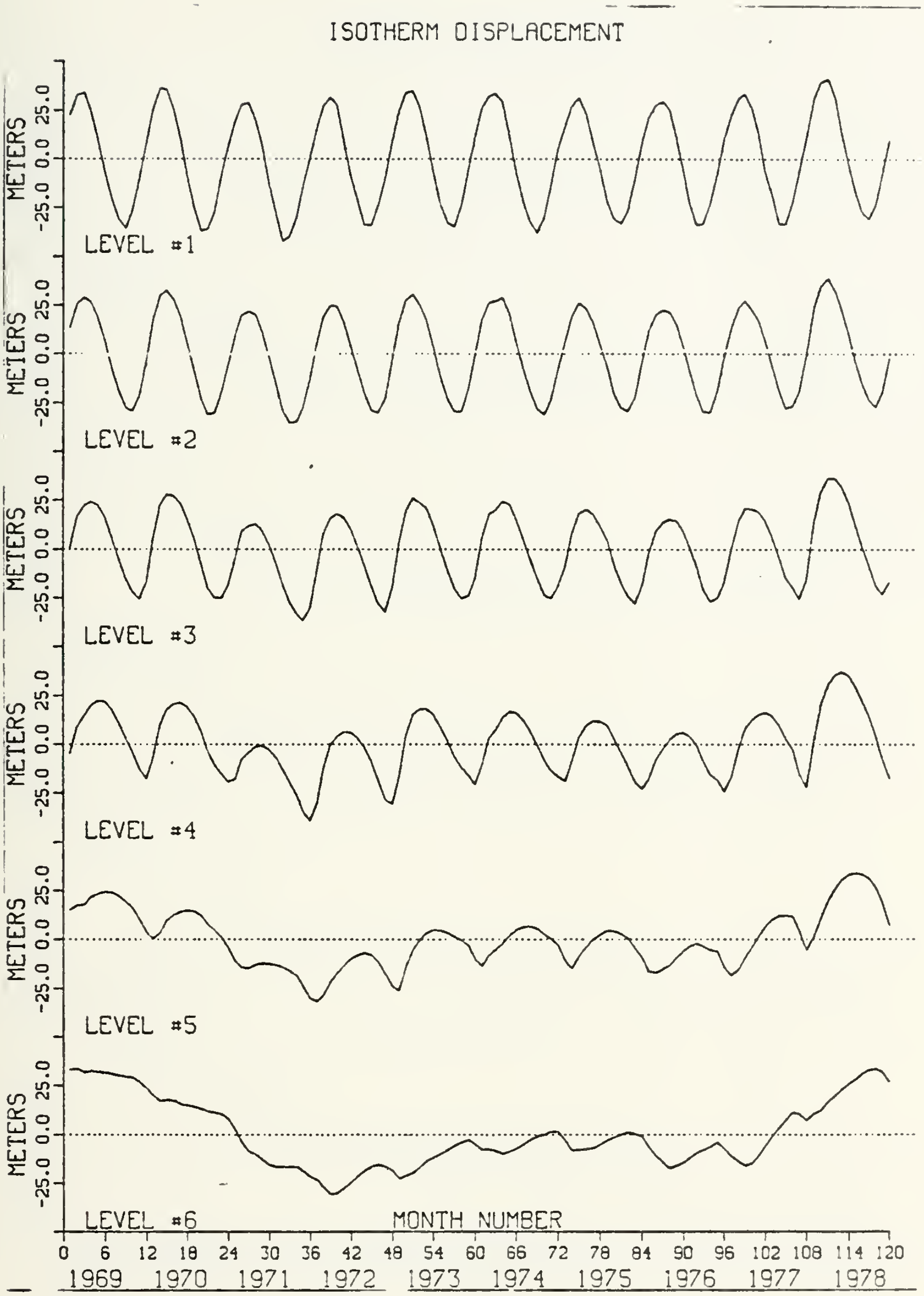

Level 1 = 5.0 m Level 2 = 16.5 m Level 3 = 33.0 m
Level 4 = 49.0 m Level 5 = 71.5 m Level 6 = 100.0 m

Figure 6. Isotherm Displacement at 30.5N 139.1W for Levels 1 to 6

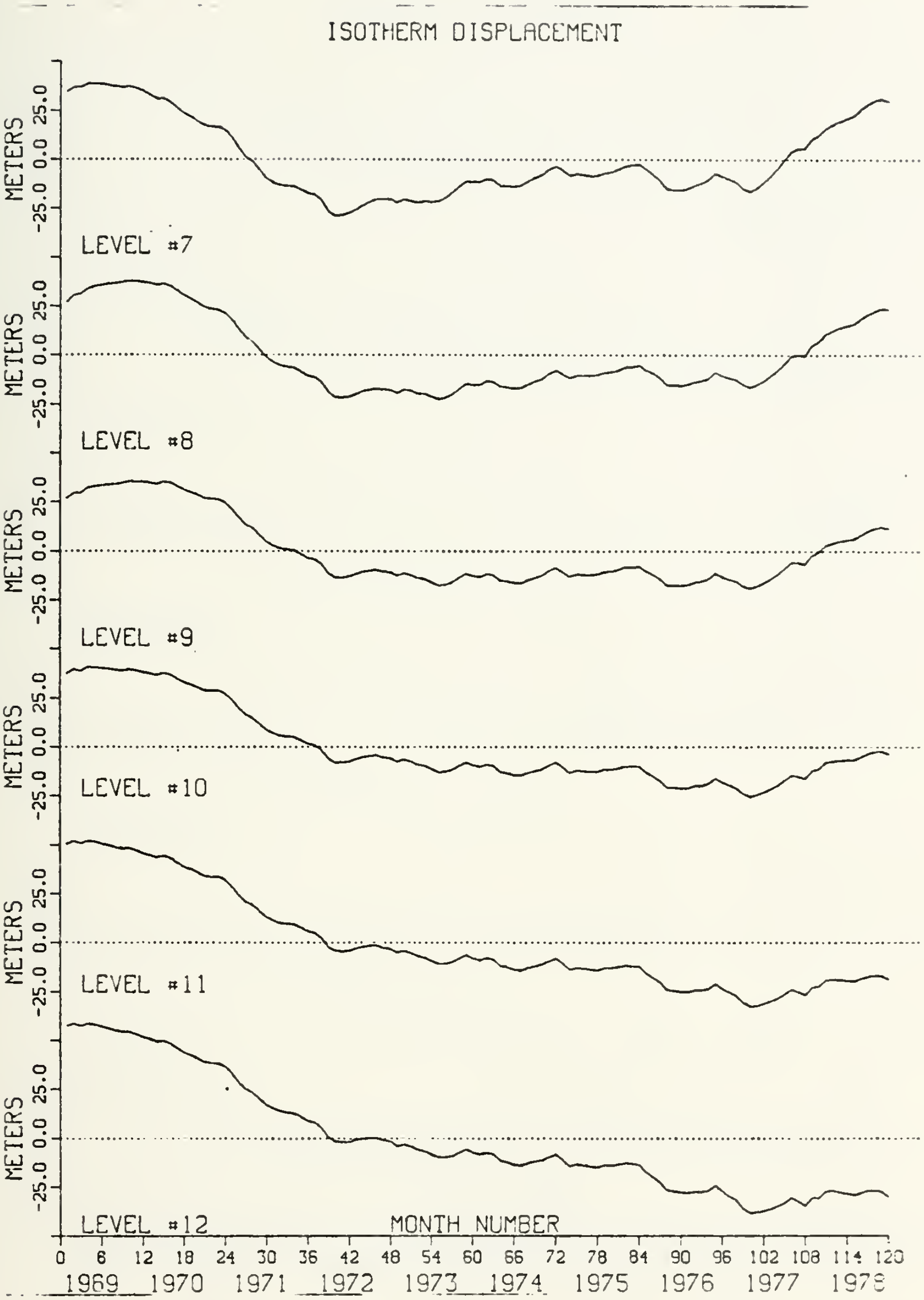

Level 7 = 136.5 m Level 8 = 182.5 m Level 9 = 240.0 m
Level 10 = 313.0 m Level 11 = 405.5 m Level 12 = 522.0 m

Figure 7. Isotherm Displacement at 30.5N 139.1W for Levels 7 to 12

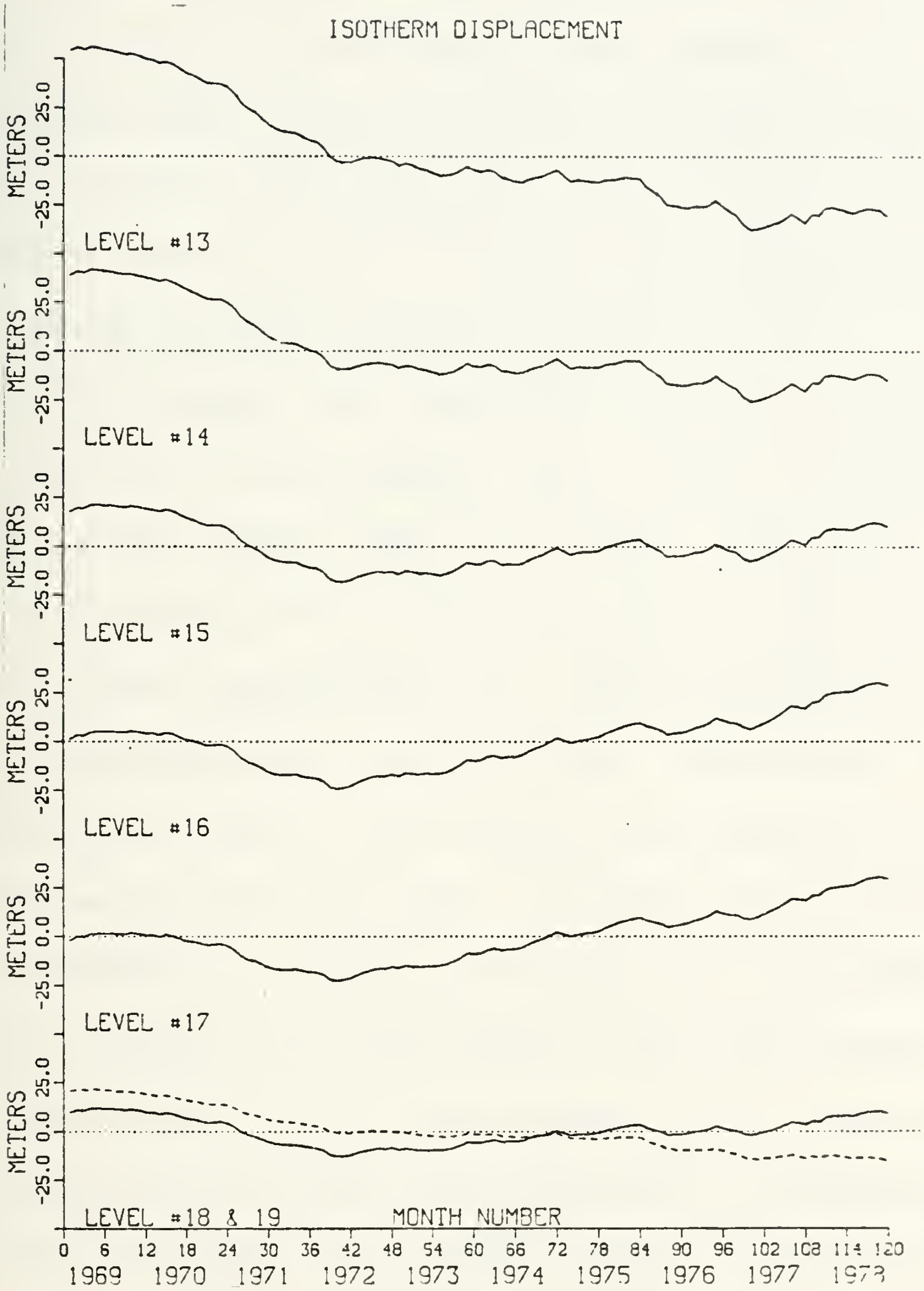

Level 19 is shown as dashed curve.

Level 13 = 669.0 m Level 14 = 855.0 m Level 15 = 1089.5 m
Level 16 = 1385.0 m Level 17 = 1760.0 m Level 18 = 2235.0 m
Level 19 = 2830.0 m

Figure 8. Isotherm Displacement at 30.5N 139.1W for Levels 13 to 19

function $c(z) = w'(z) - \phi(z)Z(z')$ are noted. In the above expression $Z(z')$ equals $w'(z')/\phi(z')$ where z' is the value of z at the bottom boundary which changes as the integration continues. Since the boundary condition states that $w'(-H) = w'(z') = 0$, then $Z(z)$ must equal zero and the c function reduces to $c(z) = w'(z)$. The eigenvalue problem thus reduces to finding values of z where $w'= 0$.

For example, for the $(\overline{N}^2)^{1/2}$ profile at 30.5N and a trial value of $\lambda = 2.5$ sec/m, $c(z) = w'(z) = 0$ when $z =$ -2451m, -1308m, -607m, -326m, and -112m. Varying λ by 0.1 sec/m, noting when $w'= 0$, and tracing out the points results in five curves (eigencurves) as shown in Figure 9. The first five eigenvalues which satisfy the boundary conditions, equations (9b), are found by the intersection of the eigencurves with the $z = 0$ line. The first five eigenvalues for this example are shown to the right of the ordinate in Figure 9; namely, $\lambda_1 = 0.4735$ sec/m, $\lambda_2 = 0.8934$ sec/m, $\lambda_3 = 1.3380$ sec/m, $\lambda_4 = 1.7814$ sec/m, $\lambda_5 = 2.1823$ sec/m. Justification for limiting the calculation of eigenvalues to the first five modes will be made apparent in the next chapter. An advantage in finding the eigenvalues in this manner is that the depth to the sea bottom need not be fixed. If

the depth to the bottom were, for example, 3 km rather than 4 km, the eigenvalues satisfying the same given boundary conditions could be obtained by noting the value of at the intersection of the eigencurves and the z = -1000 m line. The reciprocal eigenvalues, c_n which correspond to the internal phase speeds in the absence of rotation associated with each baroclinic mode, are given in Table I for the latitudes of each selected grid point. The tabular values of c_n show a decrease with latitude and with increasing mode number.

Using expendable bathythermograph (XBT) data taken at weather station November (30N, 140W) during July 1966 to December 1969, Emery and Magaard (1976) obtained c_n values of c_1 = 2.99 m/sec, c_2 = 1.41 m/sec, c_3 = 0.92 m/sec, c_4 = 0.72 m/sec, and c_5 = 0.51 m/sec. These values are slightly higher than the values given in Table I for latitude 30.5N (latitude of model grid point closest to the latitude of weather station November). The difference can be attributed to the deeper depth at weather station November (4755 m) and to larger values for N^2 (i.e., the values for N^2 calculated from the model simulated temperature field is smaller than observed).

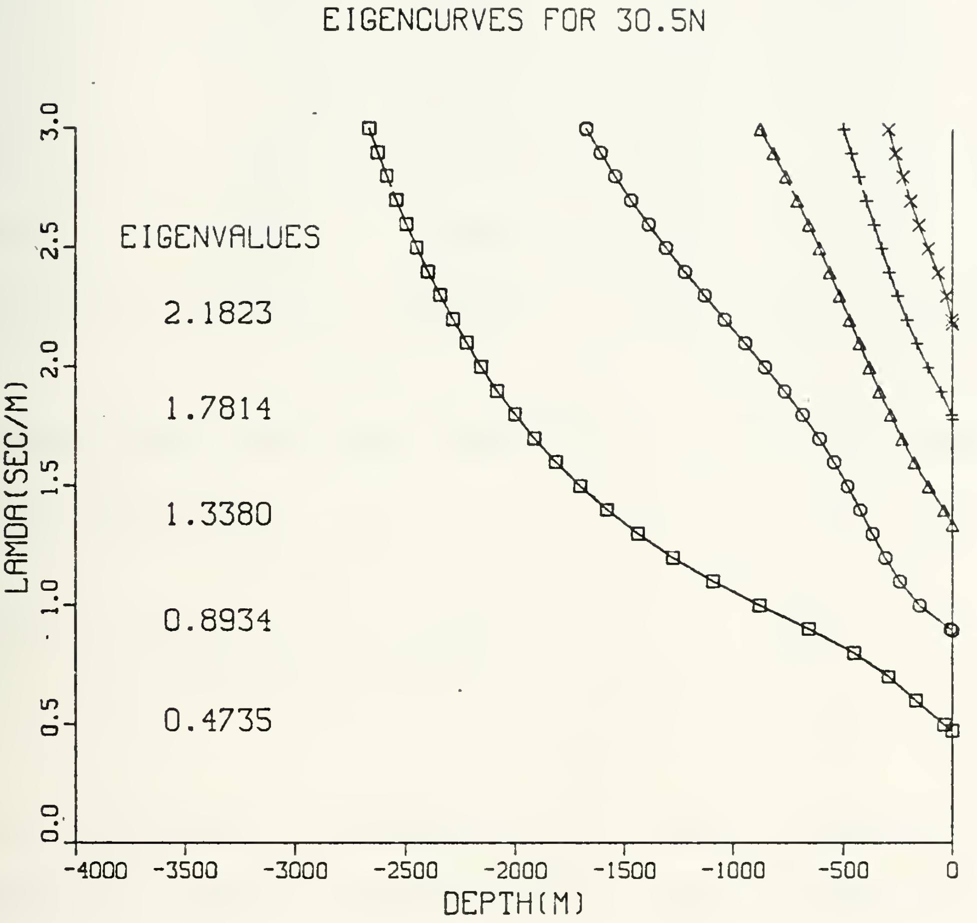

Figure 9. Eigencurves and Eigenvalues for Latitude 30.5N

Having determined the first five eigenvalues by the "c-root method", the next step is to calculate the corresponding eigenfunctions, w'_n , using IODE. The

TABLE I

Reciprocal Eigenvalues(m/sec) for Modes 1 to 5

LATITUDE	MODE NUMBER 1	2	3	4	5
18.3N	2.2578	1.2442	0.8505	0.6274	0.5049
24.4N	2.2331	1.1966	0.8202	0.6099	0.4922
30.5N	2.1119	1.1193	0.7474	0.5614	0.4582
36.6N	1.7937	0.9774	0.6245	0.4719	0.3883
42.7N	1.3289	0.7510	0.4736	0.3620	0.3077
48.8N	0.9299	0.4831	0.3294	0.2629	0.2264
54.8N	0.5511	0.2598	0.2153	0.1722	0.1356

eigenfunctions are then normalized, following Emery and Magaard (1976), as

$$\gamma_n(z) = \frac{w_n'(z)}{\left[\int_{-H}^{o} \bar{N}^2(z)(w_n'(z))^2 dz\right]^{1/2}}, \qquad (16)$$

where n represents the mode number. Since equation set (9) represents a Sturm-Liouville system, the eigenfunctions are orthogonal with respect to the weight function $\bar{N}^2(z)$ over the vertical column z = -H to z = 0, *viz.*,

$$\int_{-H}^{o} \bar{N}^2(z) w_n'(z) w_m'(z) dz = 0 \; ; \quad n \neq m \qquad (17)$$

Therefore, normalization of the eigenfunctions results in the orthonormal set, $\{\gamma_n\}$, viz.,

$$\int_{-H}^{0} \overline{N}^2(z)\gamma_n(z)\gamma_m(z)\,dz = \delta_{nm} , \qquad (18)$$

where δ_{nm} is the Kronecker delta function. A more detailed discussion concerning the orthogonality condition for the eigenfunctions is given by Willmott and Mysak (1980). The normalized eigenfunctions for the selected latitudes are shown in Figures 10 through 16. The characteristics of the eigenfunctions are related to the profile of $\overline{N}^2$ (z). At latitudes south of 40N (Figures 10 to 13) the nodal points of the normalized eigenfunctions are concentrated near the upper half of the column in response to the model simulated upper ocean $\overline{N}^2$ maximum (maximum temperature gradient). At the northern latitudes (Figures 15 and 16), the normalized eigenfunctions are very nearly sinusoidal, particularly at the higher modes. This corresponds to the near constant profile of $(\overline{N}^2)^{1/2}$ (Figures 4 and 5) below 150 m.

The analysis procedure is concluded by fitting the normalized eigenfunctions to the simulated isotherm displacement, D(z,t). This is done in the time domain by

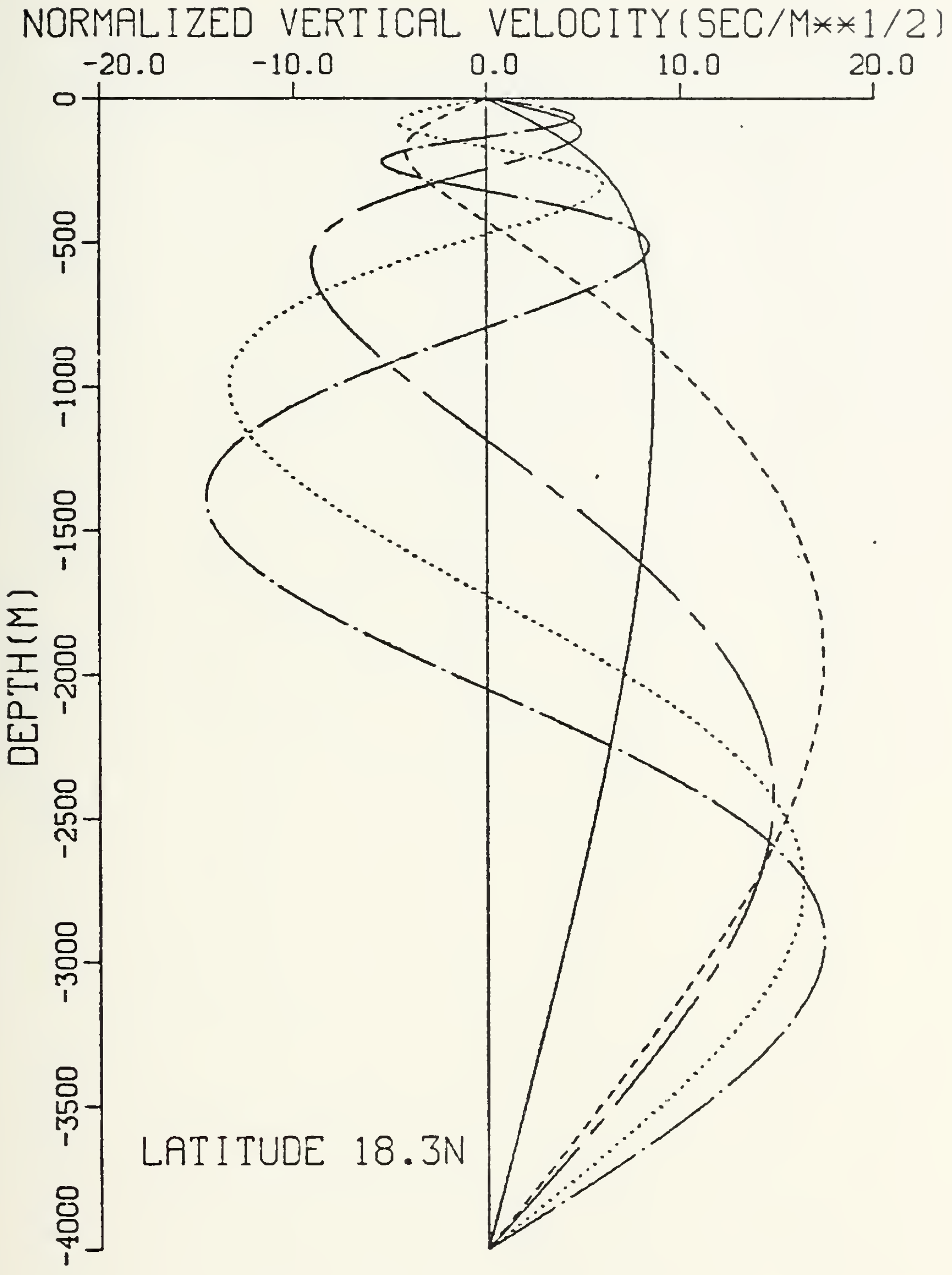

Mode 1: Solid; Mode 2: Dashed; Mode 3: Long dash/Short dash; Mode 4: Dotted; Mode 5: Long dash/Dot

Figure 10. Normalized Eigenfunctions at 18.3N

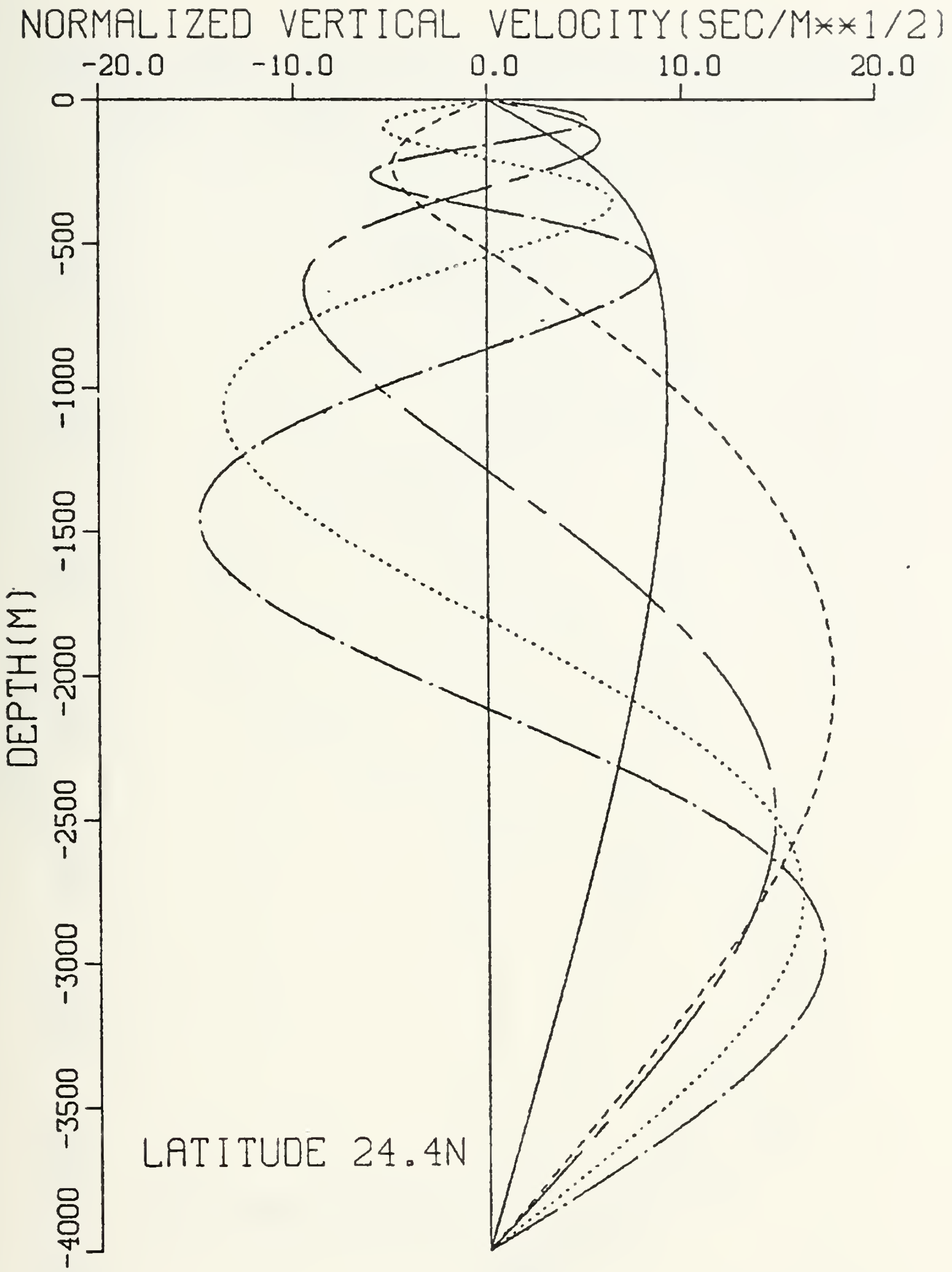

Mode 1: Solid; Mode 2: Dashed; Mode 3: Long dash/Short dash;
Mode 4: Dotted; Mode 5: Long dash/Dot

Figure 11. Normalized Eigenfunctions at 24.4N

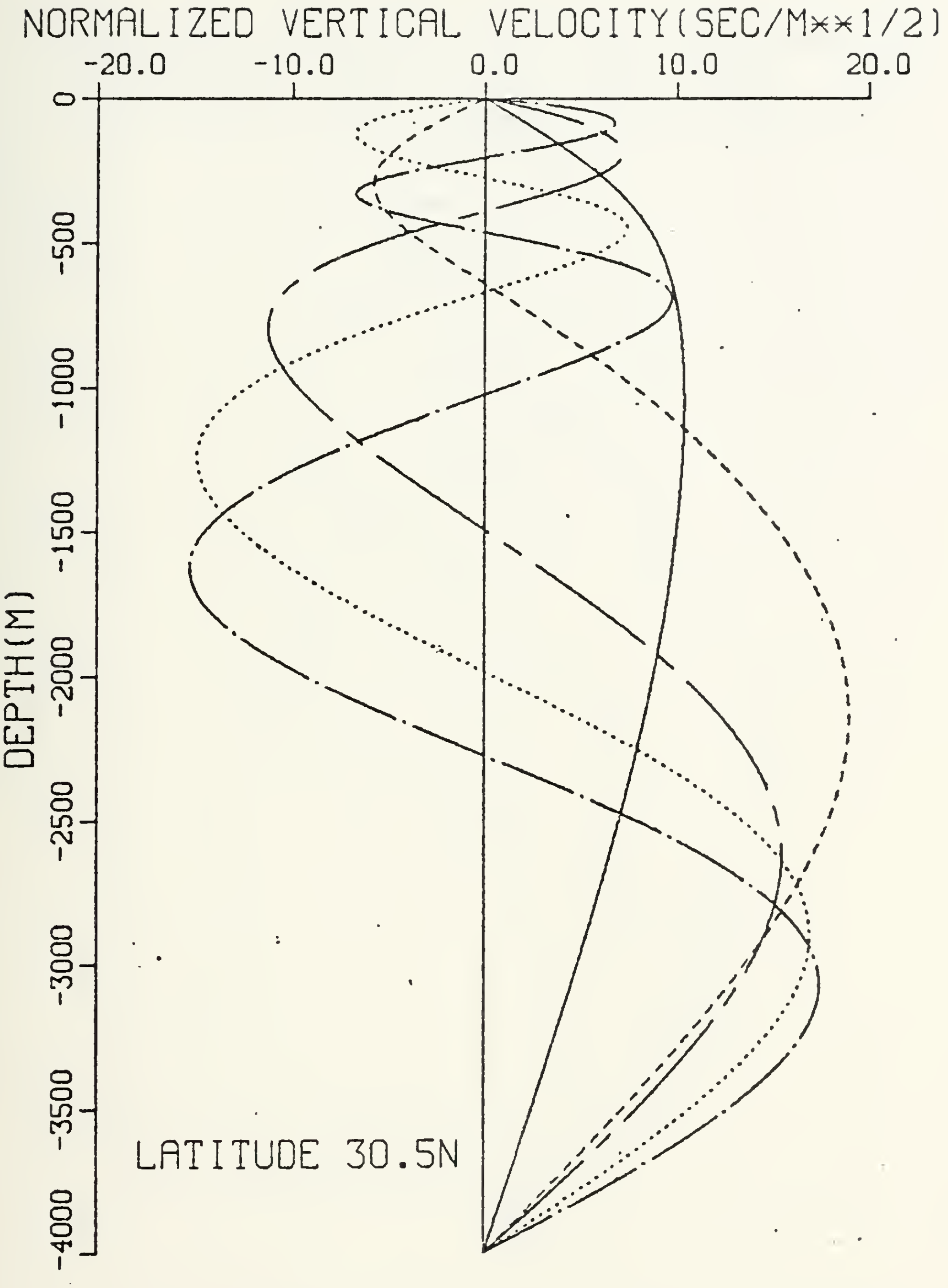

Mode 1: Solid; Mode 2: Dashed; Mode 3: Long dash/Short dash;
Mode 4: Dotted; Mode 5: Long dash/Dot

Figure 12. Normalized Eigenfunctions at 30.5N

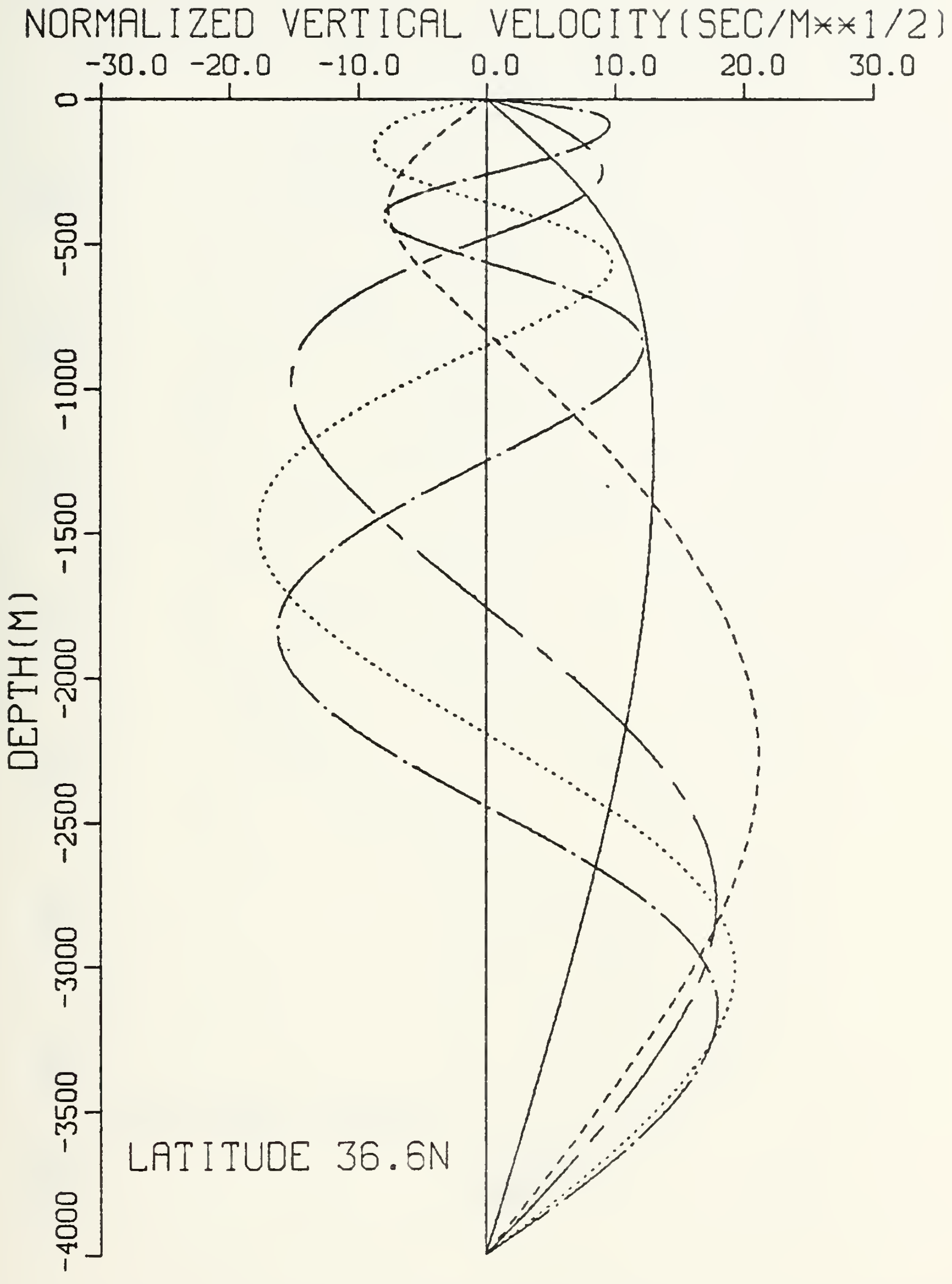

Mode 1: Solid; Mode 2: Dashed; Mode 3: Long dash/Short dash; Mode 4: Dotted; Mode 5: Long dash/Dot

Figure 13. Normalized Eigenfunctions at 36.6N

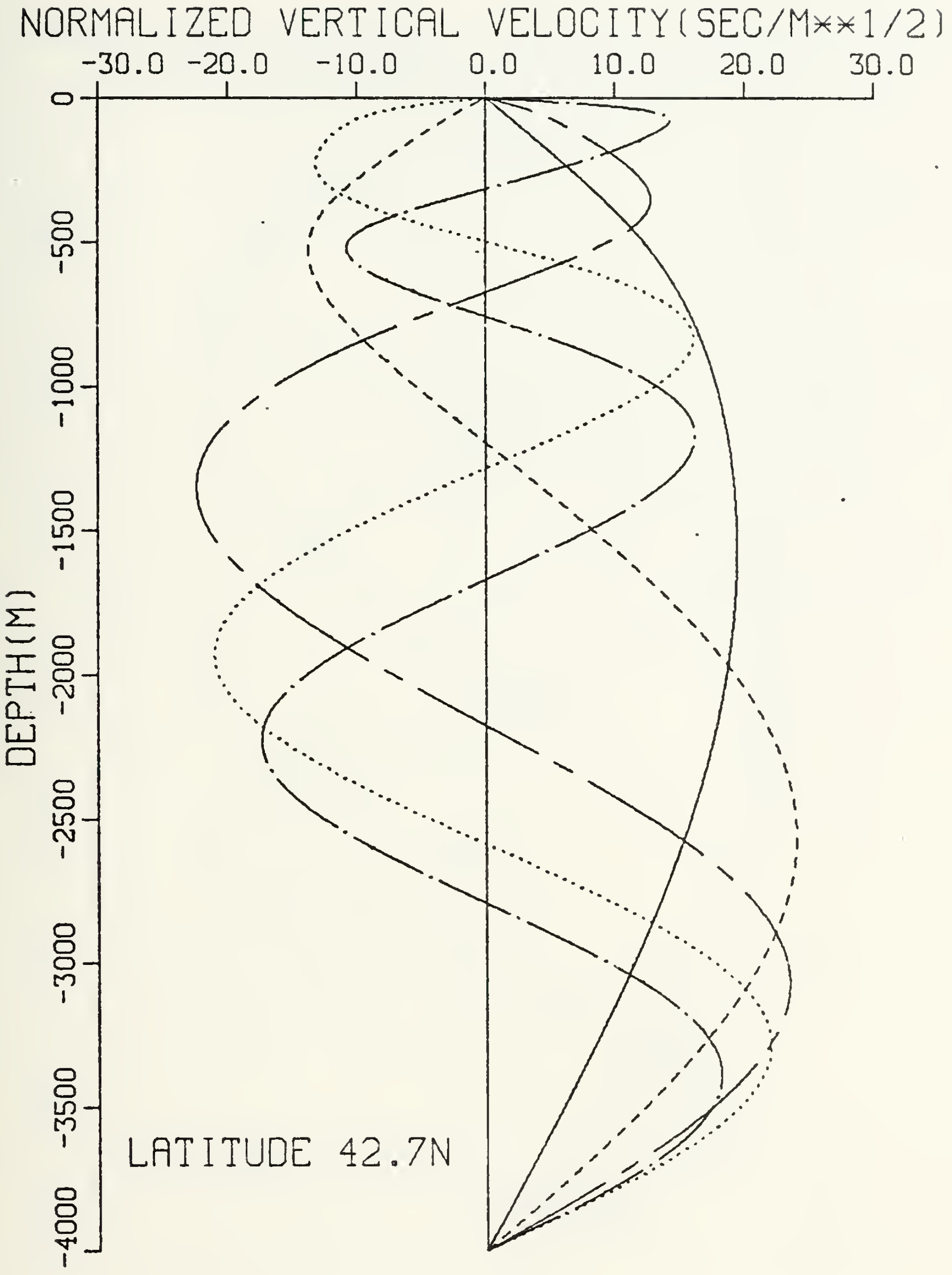

Mode 1: Solid; Mode 2: Dashed; Mode 3: Long dash/Short dash; Mode 4: Dotted; Mode 5: Long dash/Dot

Figure 14. Normalized Eigenfunctions at 42.7N

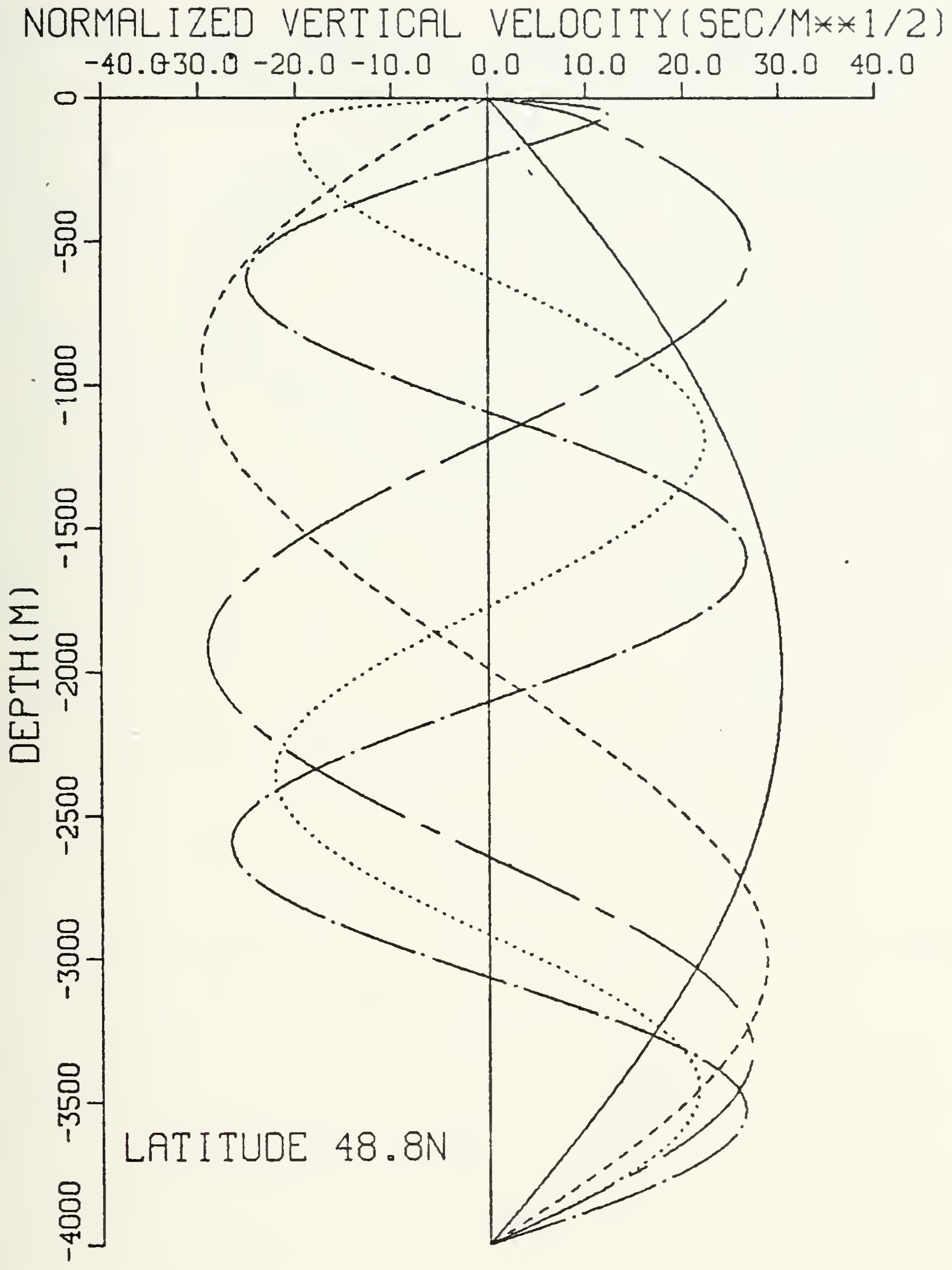

Mode 1: Solid; Mode 2: Dashed; Mode 3: Long dash/Short dash; Mode 4: Dotted; Mode 5: Long dash/Dot

Figure 15. Normalized Eigenfunctions at 48.8N

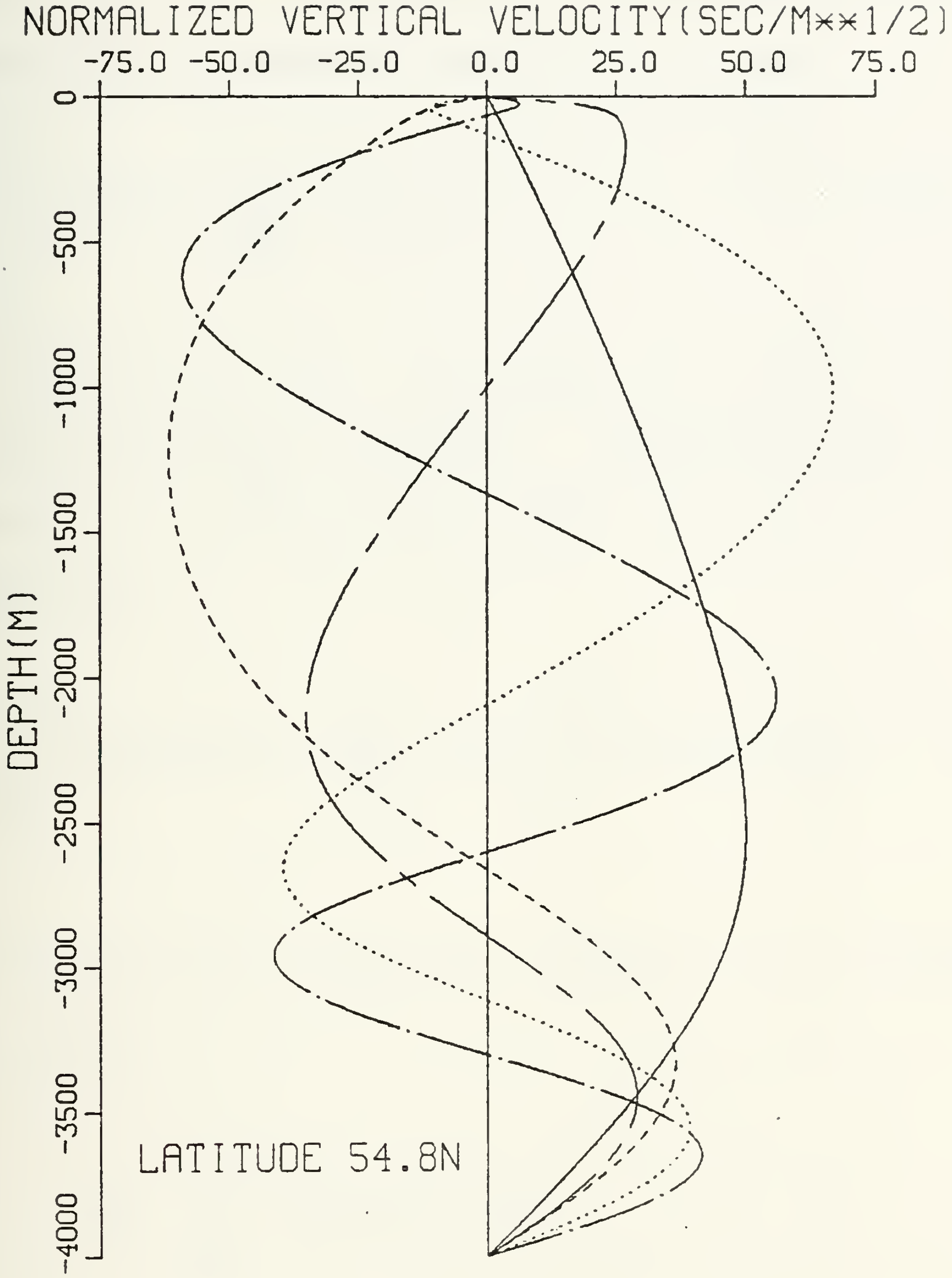

Mode 1: Solid; Mode 2: Dashed; Mode 3: Long dash/Short dash;
Mode 4: Dotted; Mode 5: Long dash/Dot

Figure 16. Normalized Eigenfunctions at 54.8N

making use of the completeness of the eigenfunctions to equate D(z,t) to the sum of the normalized eigenfunctions multiplied by an amplitude coefficient A_n, viz.,

$$D(z,t) = \sum_{n=1}^{\infty} A_n(t)\gamma_n(z) . \qquad (19)$$

The coefficients, $A_n(t)$, are readily obtained by making use of the orthonormality condition. Multiplying each side of equation (19) by $\bar{N}^2\gamma_m$ and then integrating from z = -H to z = 0 results in

$$\int_{-H}^{0} \bar{N}^2(z)\gamma_m(z)D(z,t)dz = \sum_{n=1}^{\infty} [A_n(t) \int_{-H}^{0} \bar{N}^2(z)\gamma_n(z)\gamma_m(z)dz] . \qquad (20)$$

Application of the othogonality condition (18) to equation (20) yields

$$A_n(t) = \int_{-H}^{0} \bar{N}^2(z)\gamma_n(z)D(z,t)dz . \qquad (21)$$

Equation (21) is used to compute $A_n(t)$ for the first five modes for each selected grid point. The deviation from the modal fit, as defined by Emery and Magaard (1976), eqn.(22),

is also calculated. The deviation term quantitatively shows how well the model simulated isotherm displacement fluctuations are fit by the first five baroclinic modes. A value of DEV(t) = 0 implies that the isotherm displacement fluctuations can be fully explained by the first five baroclinic modes.

$$\mathrm{DEV}(t) = \frac{\displaystyle\int_{-H}^{0} \bar{N}^2(z)\Big[D(z,t) - \sum_{n=1}^{5} A_n(t)\gamma_n(z)\Big]^2 dz}{\displaystyle\int_{-H}^{0} \bar{N}^2(z)\, D^2(z,t)\,dz} \,. \qquad (22)$$

III. RESULTS

The coefficients, $A_n(t)$, and the deviation, DEV(t), calculated at each selected grid point are shown in Figures 17 to 24. At lower latitudes (Figures 17 to 19 and Figure 24) the amplitude of coefficient A_1 is generally larger than the coefficients A_2 to A_5 indicating the importance of the first mode at the southern latitudes. At latitude 24.4N (Figure 18) a seasonal signal is evident for coefficients A_4 and A_5. The seasonal signal of the higher modes becomes more apparent with increasing latitude indicating that the seasonally varying model input parameters appear to be reflected in the higher modes at higher latitudes. At the northern most grid point, 54.8N (Figure 23) the overall amplitude increases an order of magnitude. Additionally, the pattern of each coefficient appears nearly identical with only slight differences in magnitude.

The deviation term at latitudes 18.3N and 24.4N remains generally below 50% during most of the ten-year model run, although some time periods are higher. North of 24.4N there is a general increase over the ten-year period in the

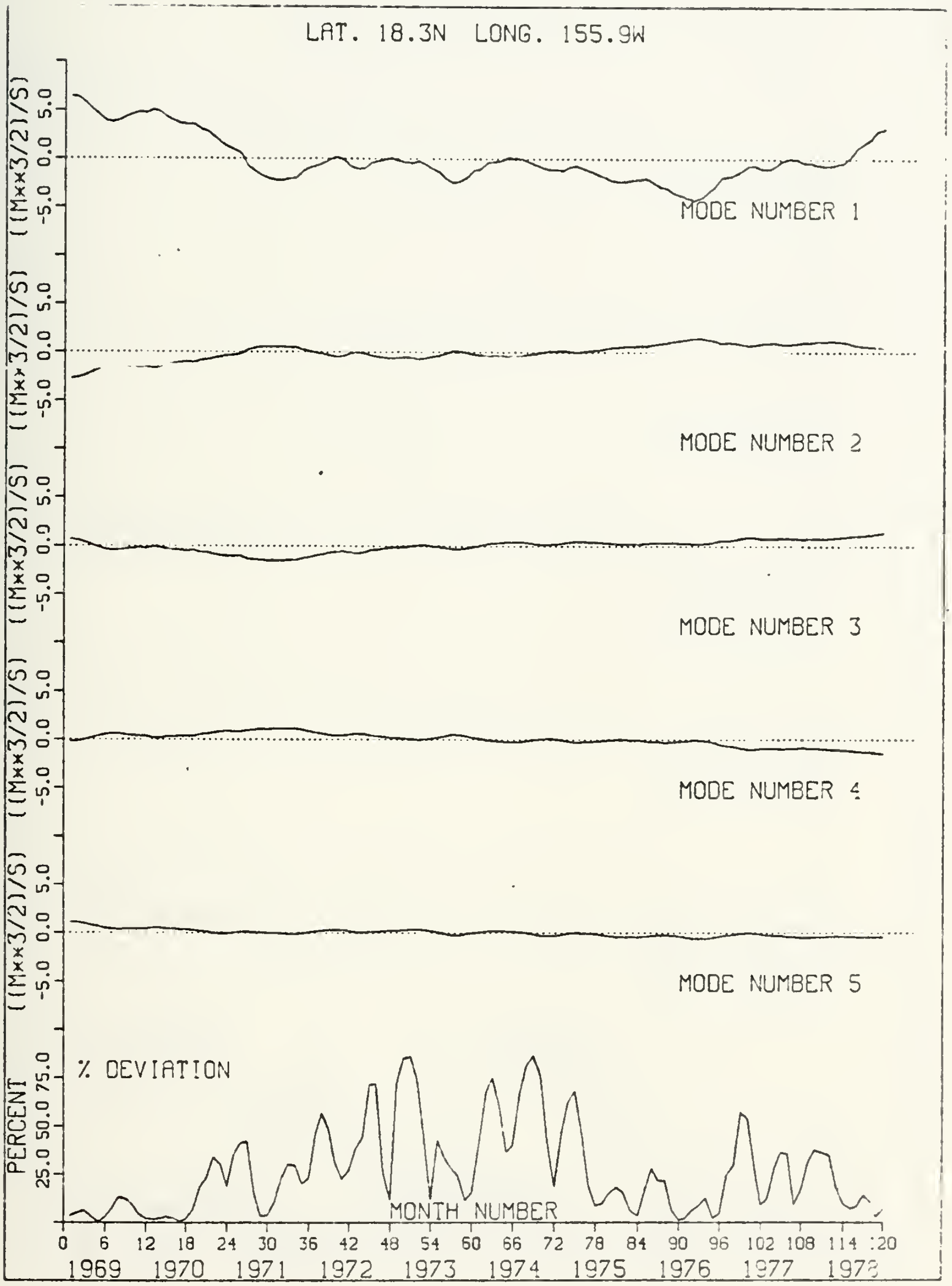

Figure 17. $A_n(t)$ and DEV(t) at 18.3N 155.9W

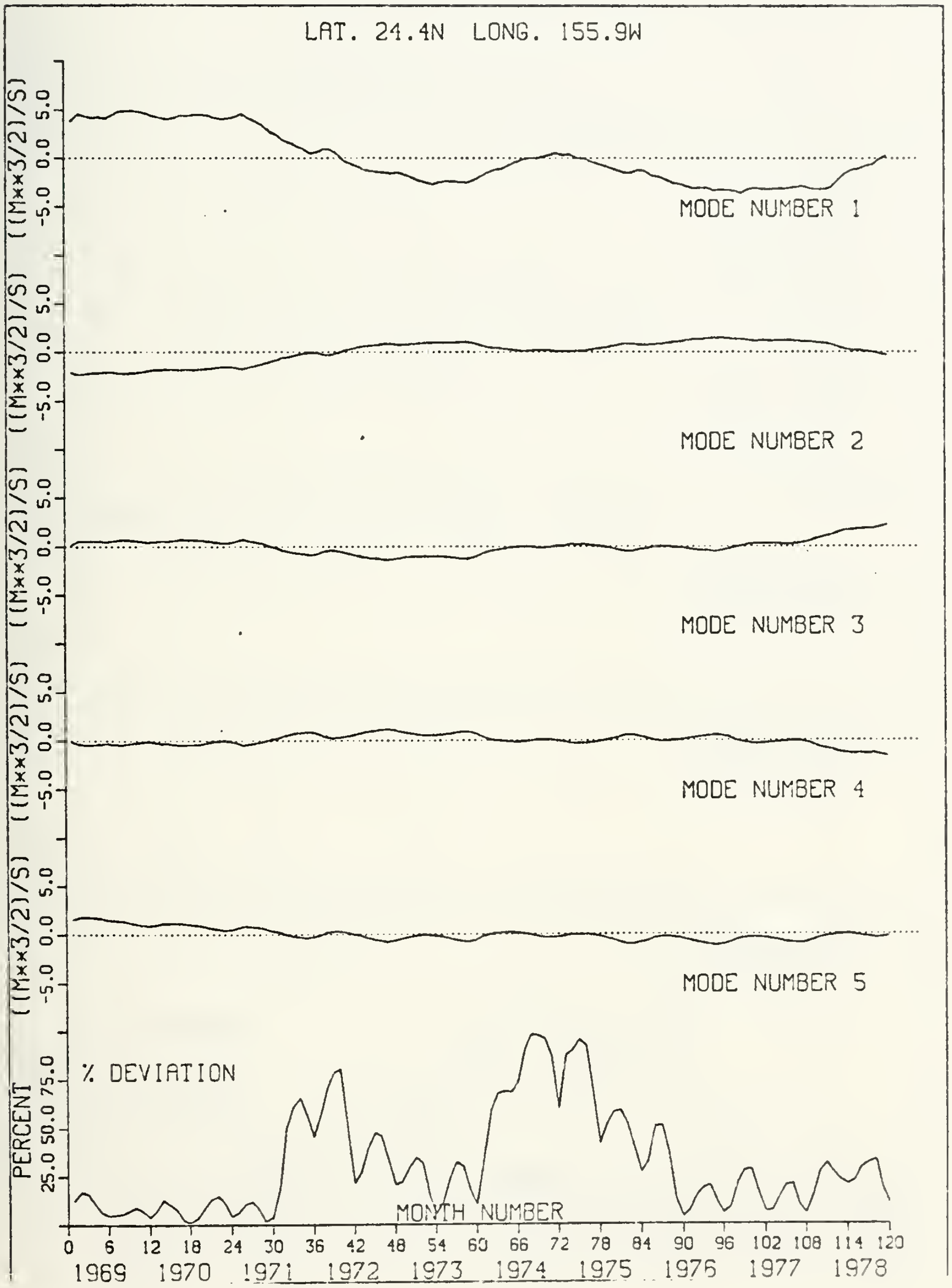

Figure 18. $A_n(t)$ and DEV(t) at 24.4N 155.9W

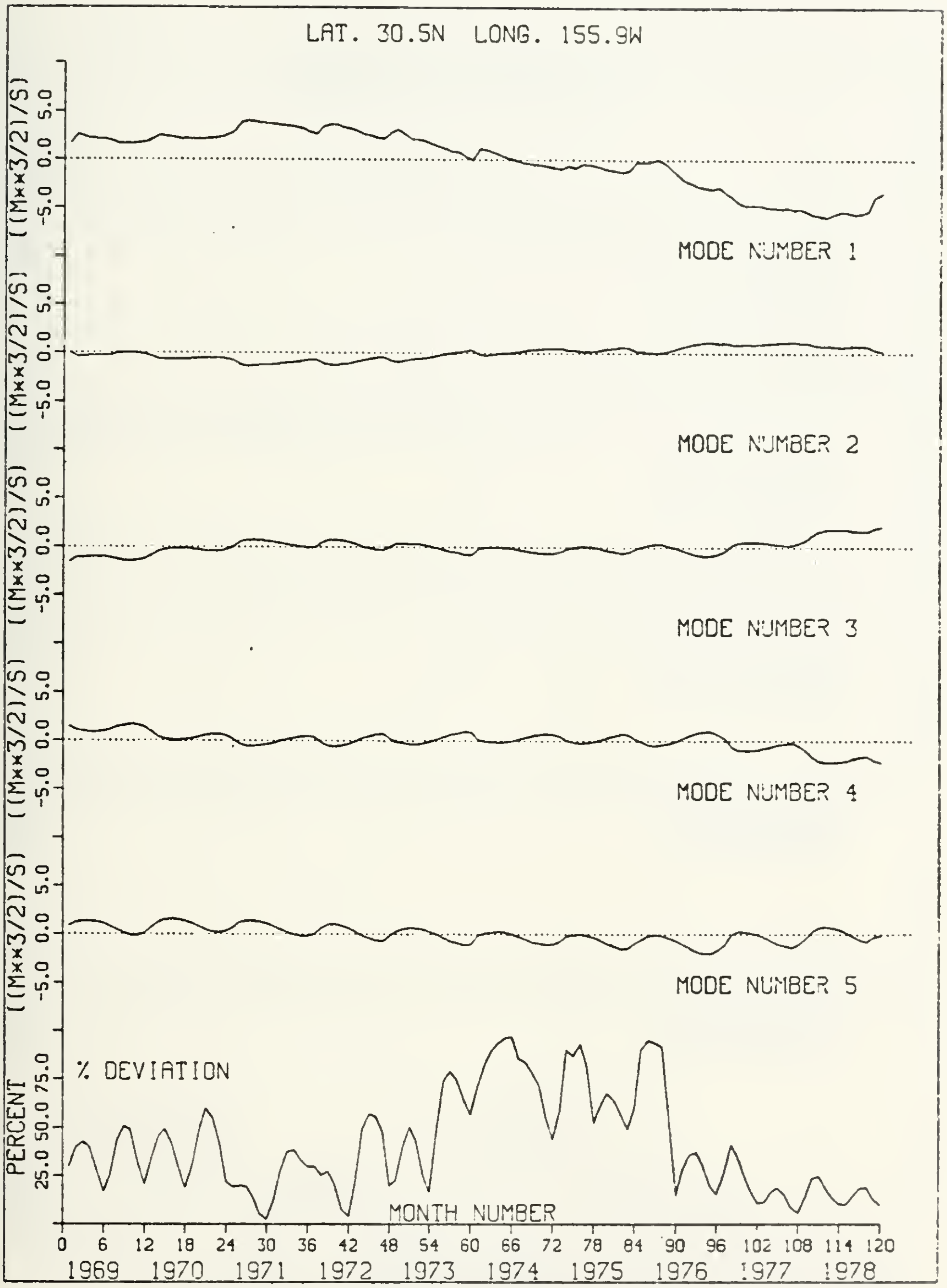

Figure 19. $A_n(t)$ and DEV(t) at 30.5N 155.9W

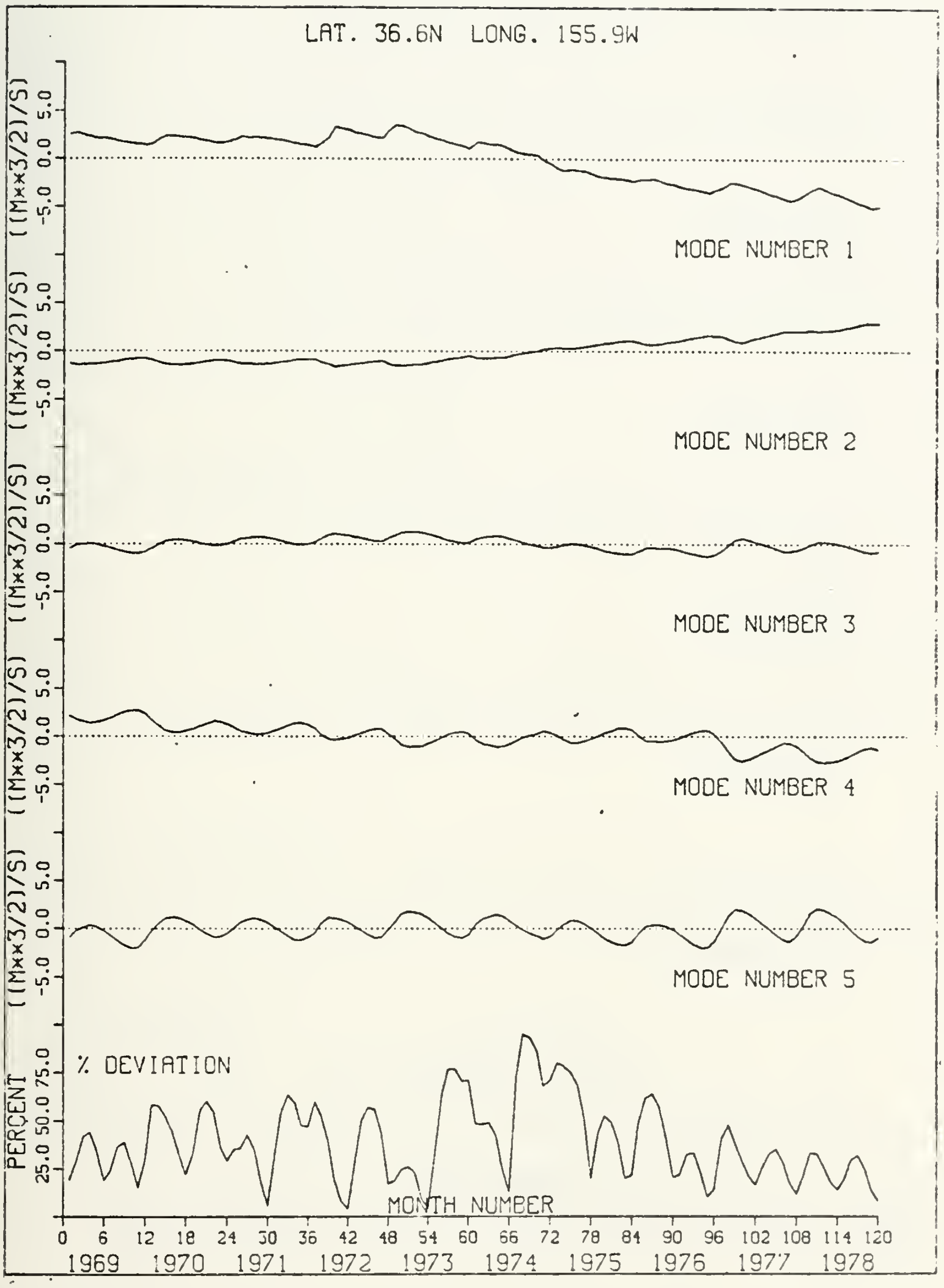

Figure 20. $A_n(t)$ and DEV(t) at 36.6N 155.9W

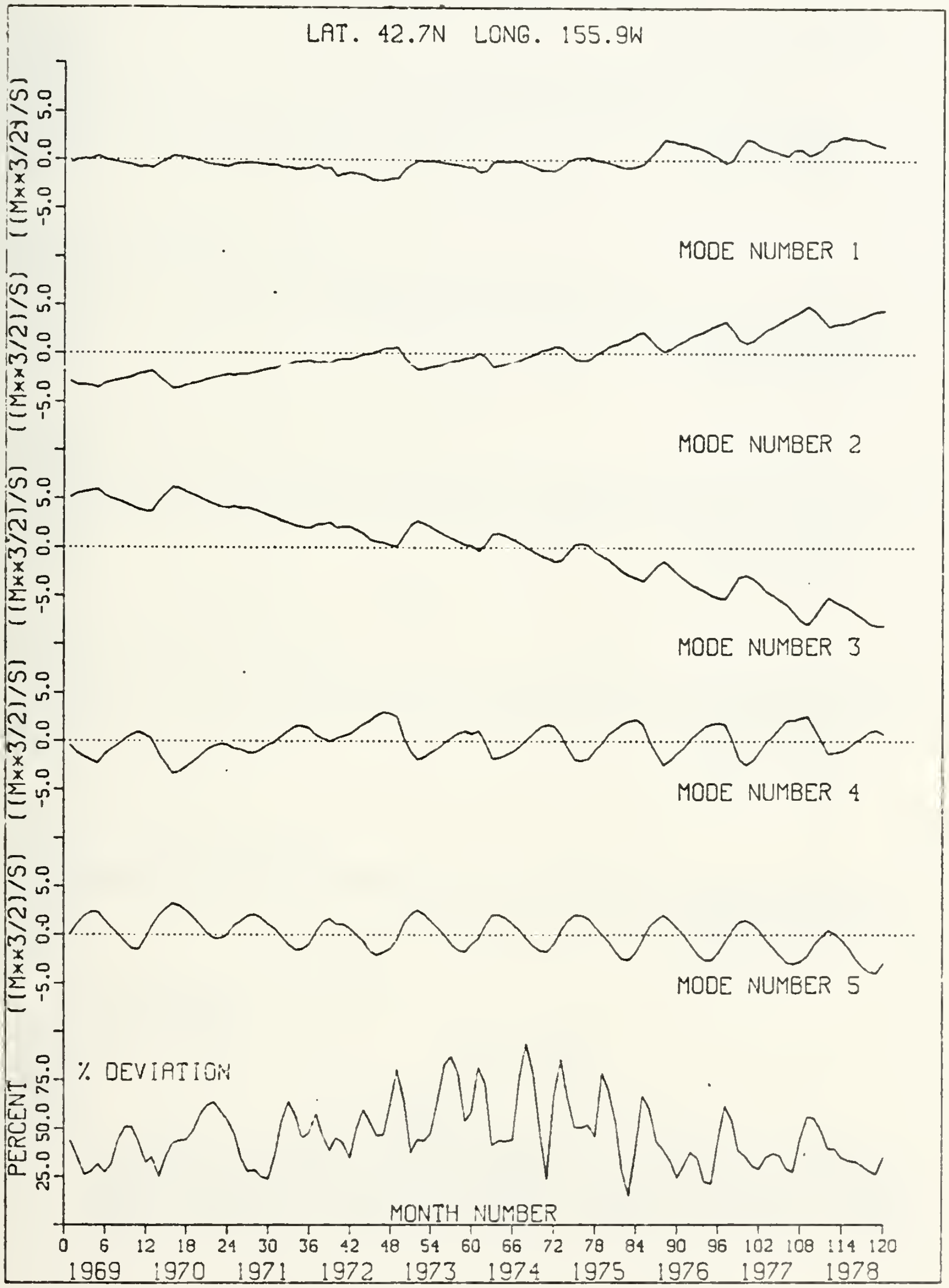

Figure 21. $A_n(t)$ and DEV(t) at 42.7N 155.9W

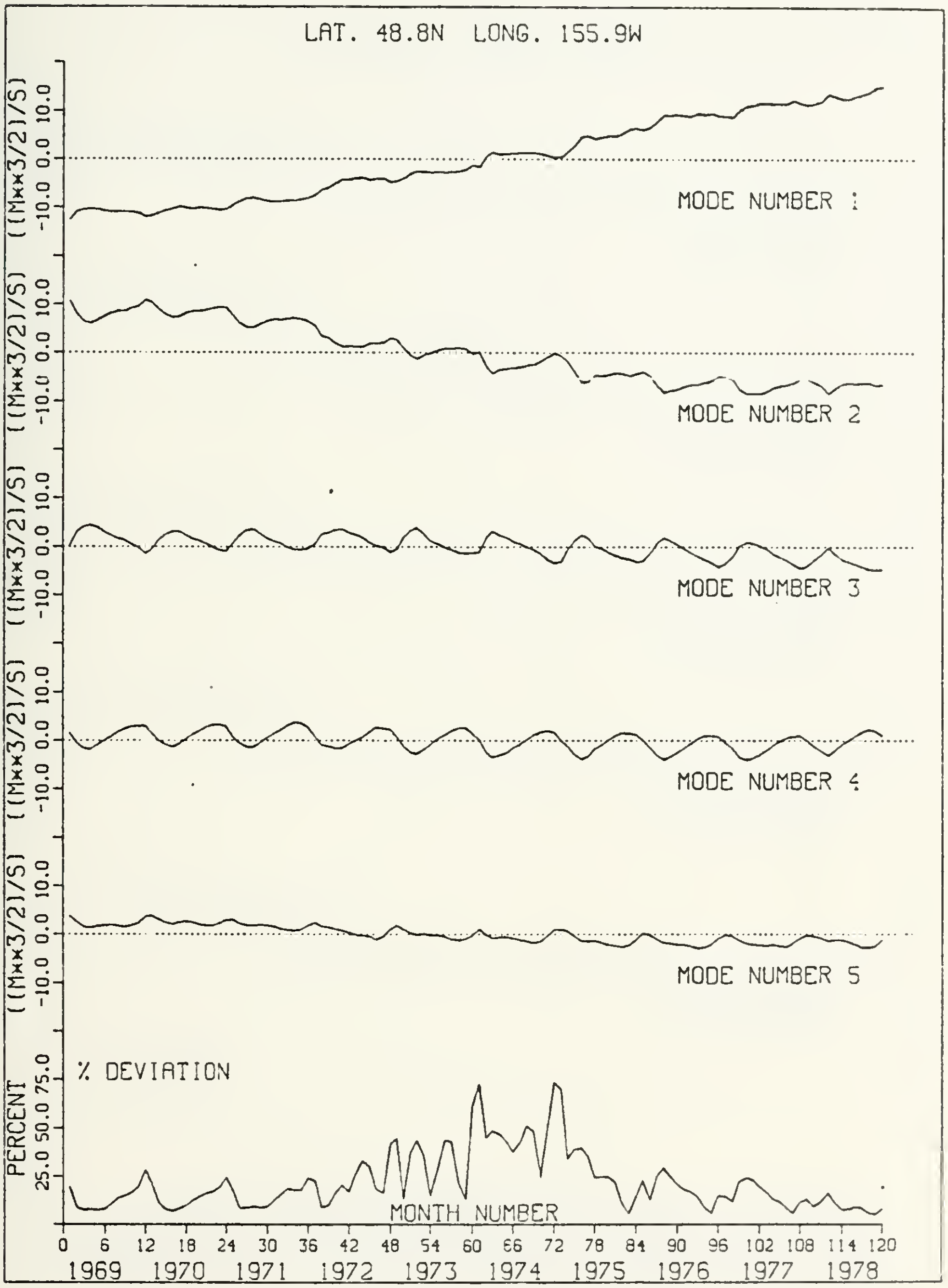

Figure 22. $A_n(t)$ and DEV(t) at 48.8N 155.9W

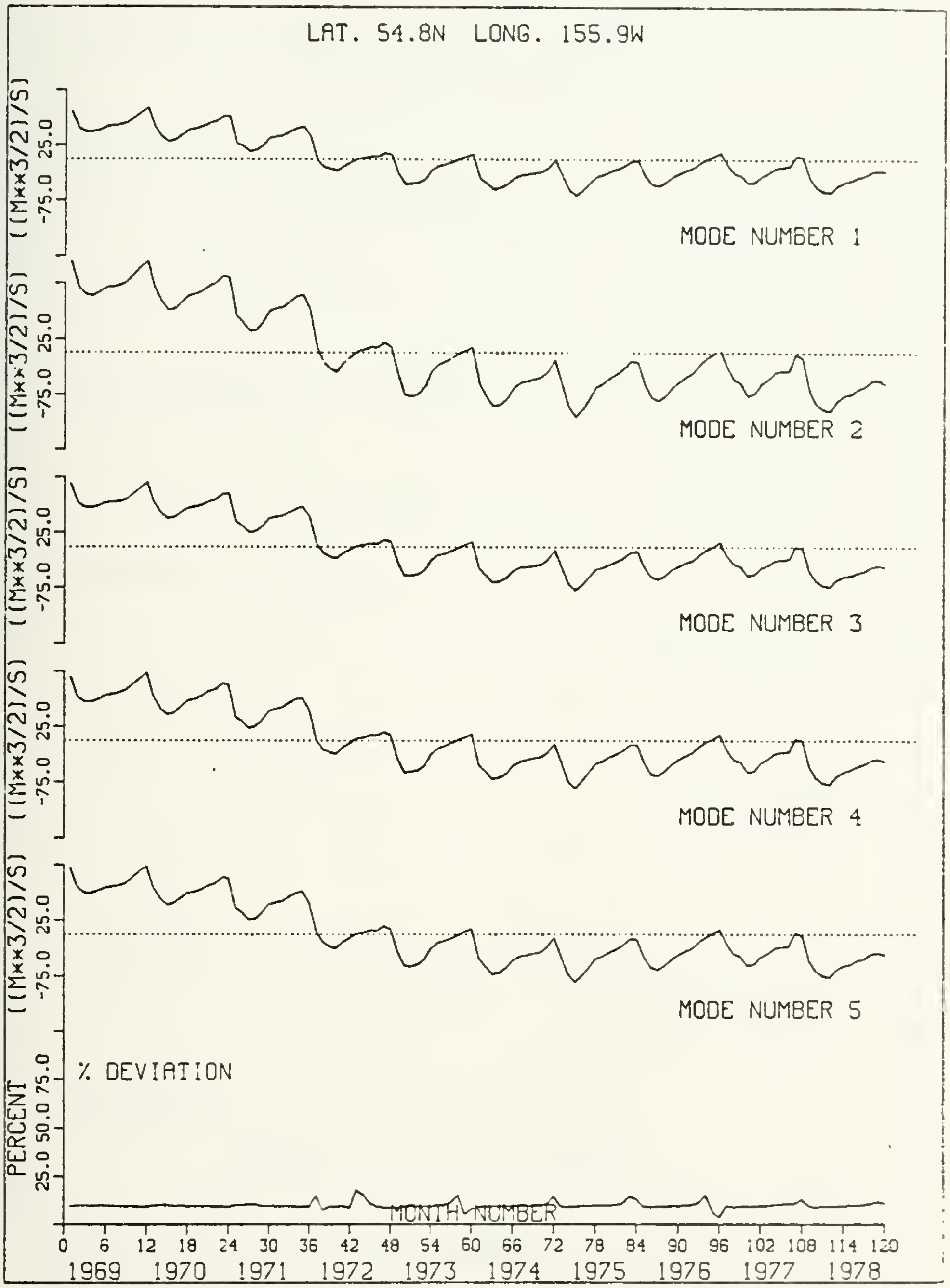

Figure 23. $A_n(t)$ and DEV(t) at 54.8N 155.9W

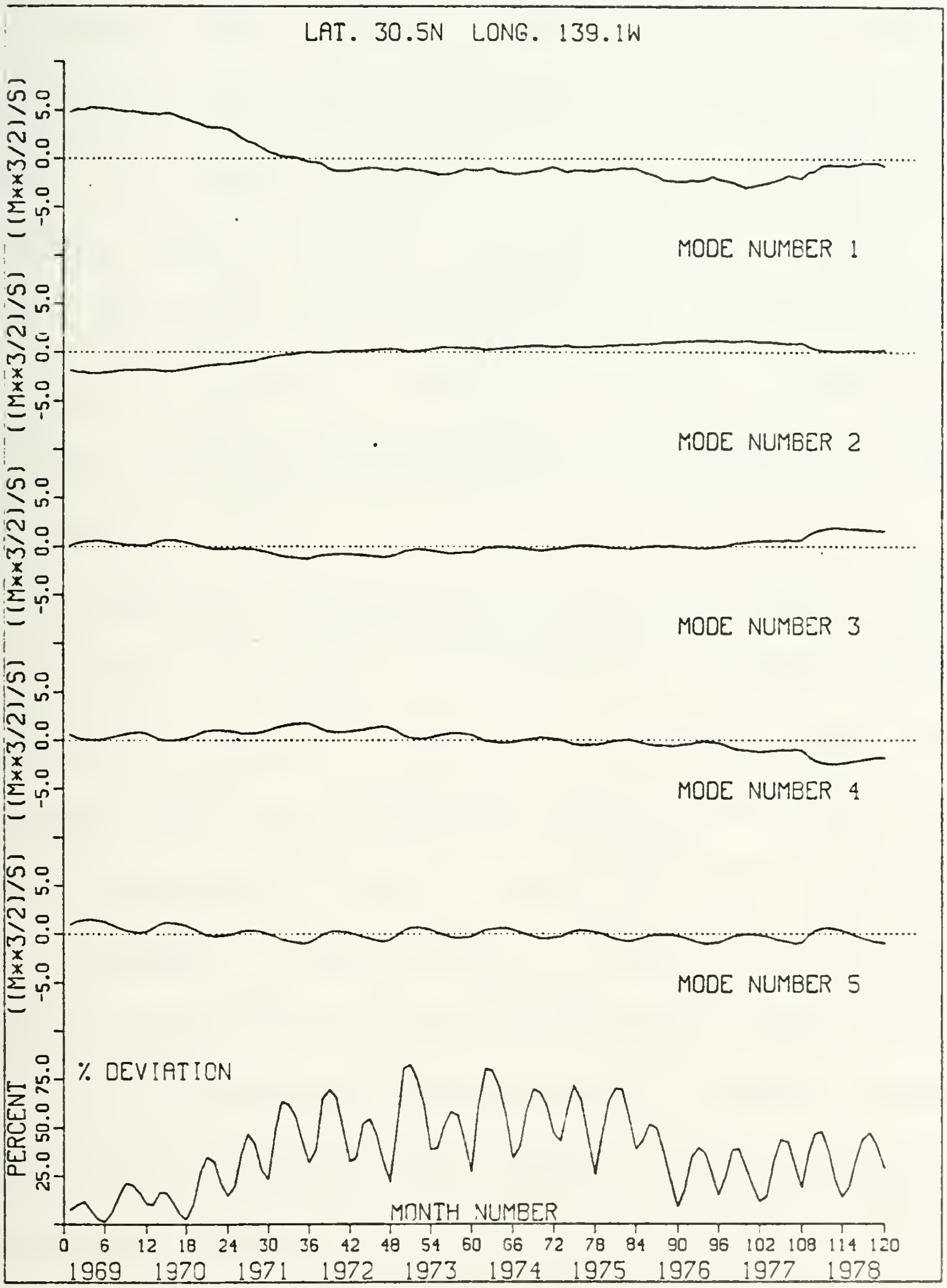

Figure 24. $A_n(t)$ and DEV(t) at 30.5N 139.1W

deviation curve with the exception of the two northern most grid points (Figures 22 and 23). As a comparison, the first five coefficients and the deviation term computed by Emery and Magaard (1976) using 48 months of data for weather station November are shown in Figure 25. The results shown in Figures 24 (model grid point closest to weather station November) and 25 compare reasonably well. Both show the largest amplitude of coefficeint A_1. The 48-month mean deviation computed for weather station November was 32% while the ten-year mean deviation is 38.2% for model grid point 30.5N 139.1W.

To examine the relative contribution made by each baroclinic mode to fitting the simulated isotherm displacement fluctuations (equation (19)), the ten-year mean deviation (equation (22)) was calculated for each selected grid point adding one mode at a time. The results are given in Table II. Column 1 (under modes) gives the ten-year mean deviation when only the first baroclinic mode is fit to the isotherm displacement fluctuations. Column 2 gives the ten-year mean deviation when modes 1 and 2 are fitted to the isotherm displacement fluctuations and so on. The tabular values show the importance of mode 1 at the selected grid

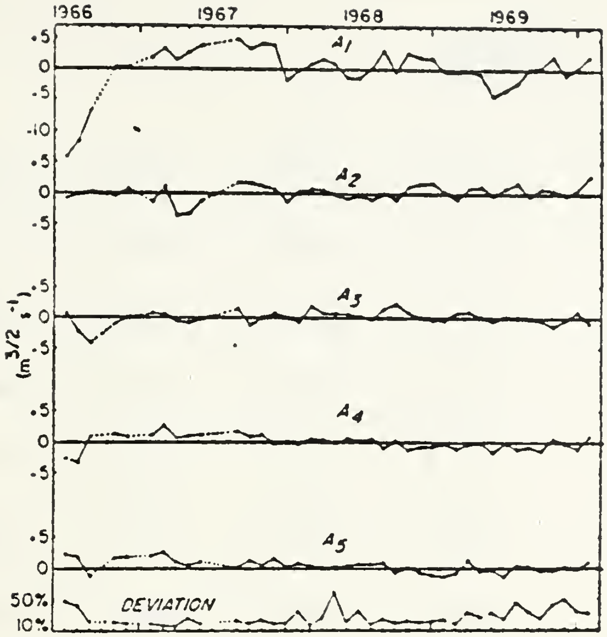

Figure 25. $A_n(t)$, and DEV(t) for weather station November (from Emery and Magaard, 1976)

points south of 30.5N (i.e., over 40% of the deviation is accounted for by the first baroclinic mode alone). The contribution made by the fifth baroclinic mode in reducing the mean deviation is less than 6% at the three southern most grid points, and, except for the northern most grid point, is less than 10% elsewhere. Based upon these results, it is apparent that adding higher baroclinic modes (modes greater than 5) would add little to reducing the deviation term compared to mode number one.

TABLE II

Mean Deviation (%) at Selected Grid Points

GRID POINT	MODES				
	1	1+2	1+2+3	1+2+3+4	1+2+3+4+5
18.3N 155.9W	56.3	46.0	36.4	28.6	26.8
24.4N 155.9W	54.1	45.9	39.0	35.0	31.6
30.5N 155.9W	57.4	54.2	50.9	46.9	41.0
36.6N 155.9W	65.2	55.7	53.3	45.3	38.8
42.7N 155.9W	96.2	88.1	60.7	54.2	46.2
48.8N 155.9W	56.1	34.5	28.8	24.1	21.6
54.8N 155.9W	90.1	57.8	43.0	26.6	10.0
30.5N 139.1W	63.6	56.5	50.9	41.1	38.2

The mean deviation (column 5 of Table II) generally increases with latitude up to 42.7N but then decreases at the two highest latitudes. Additionally, the contribution of modes 2 to 5 in reducing the mean deviation is significant at the northern most points. To examine the relevance of these results, the cutoff period (minimum period) for the propagation of free Rossby waves of mode n (see Emery and Magaard (1976)) given by $\hat{T} = (4\pi f \lambda_n)/\beta$ was evaluated. The results are shown in Figure 26. The dotted line delineates the annual period and the dashed line the five year period.

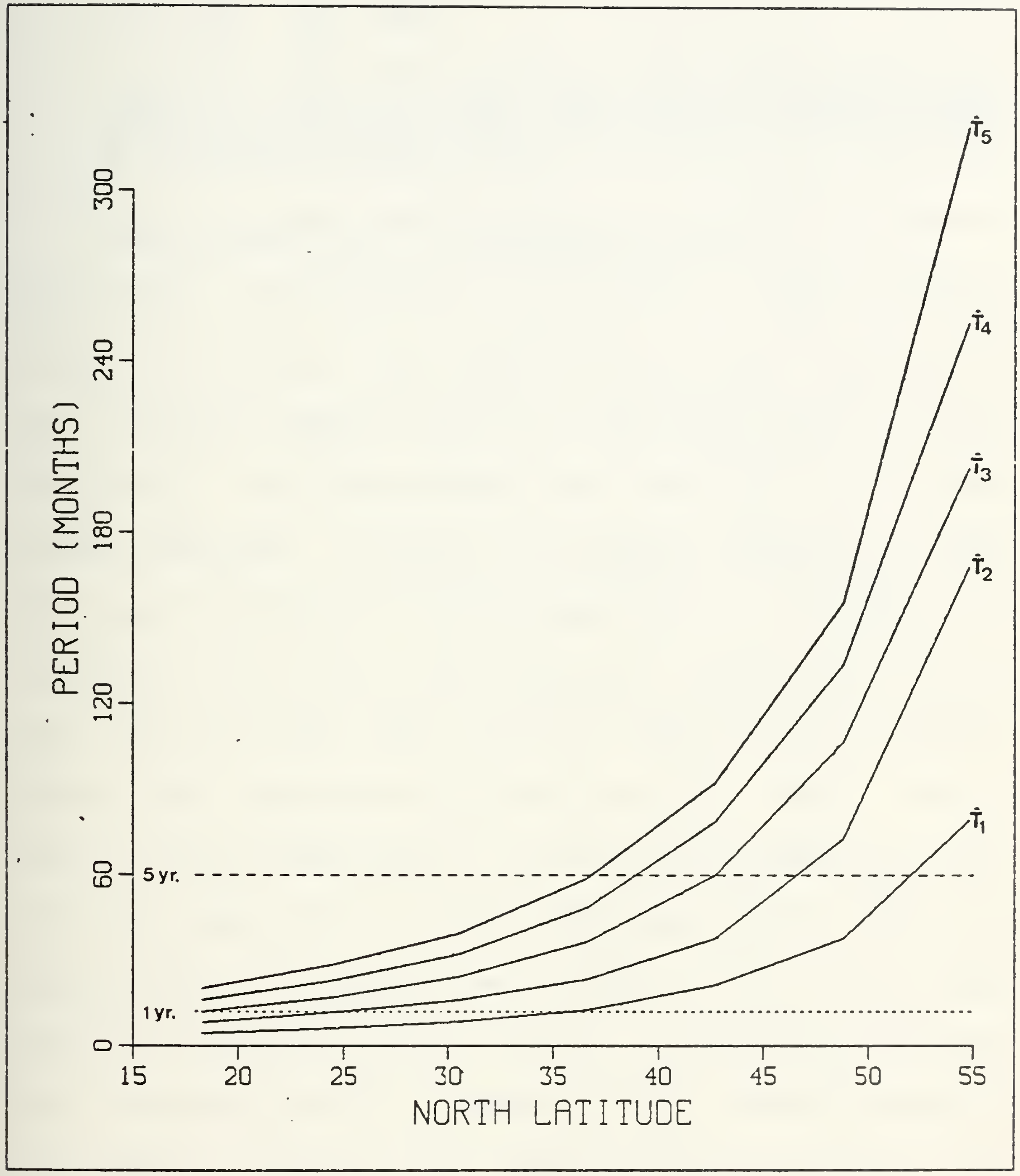

Figure 26. Cutoff Period versus Latitude

The curves of Figure 26 show the following results:

- Based upon the theoretical cutoff period annual period baroclinic free Rossby waves may exist north of 25N but only mode 1 can occur.
- Baroclinic free Rossby waves at the annual period cannot exist north of approximately 36N (recall Magaard (1983) stated that first mode baroclinic Rossby waves were primarily evident between latitudes 30 to 40 North in the North Pacific Ocean).
- Baroclinic free Rossby waves at the five year period cannot exist north of approximately 52N.

The results given above are significant. Since the free Rossby wave analysis was conducted using only ten years of model simulated temperature data, free Rossby waves of periods greater than approximately five years can not be adequately resolved. Therefore, the results obtained for model grid point 54.8N 155.9W losses significance. Likewise, at grid point 48.8N 155.9W the theoretical cutoff period curves show that only first mode baroclinic Rossby waves at periods greater than approximately three years can exist. Therefore, the low deviation at latitude 48.8N resulting primarily from modes 2 to 5 is not necessarily due to baroclinic Rossby waves. The opposite may be said of the selected grid points at latitudes 18.3N to 36.6N. At these latitudes the first baroclinic mode is dominant and the cutoff period is 4.5 months at 18.3N and 12.8 months at latitude 36.6N. At latitude 42.7N the cutoff period is 21.4 months. However,

only the first and second modes can exist at periods less than five years. The mean deviation is high when only the first and second modes are fitted to the isotherm displacement fluctuations (96.2% and 88.1% in columns 1 and 2, respectively, of Table II). Thus at model grid point 42.7N 155.9W the model simulated isotherm displacement fluctuations cannot be explained by free baroclinic Rossby waves in the time domain.

Thus far the examination of baroclinic free Rossby wave signature in the model simulated temperature field (or isotherm displacement) has been limited to the time domain only. In order to conduct an analysis of baroclinic free Rossby wave signature in the space domain requires carrying out a cross-sprectral fit of the x and y direction wave numbers at the appropriate frequencies. In the context of this study a cursory examination of the wave number vectors will be made. The locus of wave number vectors for mode 1 at appropriate frequencies for latitudes 18.3N and 36.6N are shown in Figures 27 and 28. The locus of wave numbers was determined using equation (11) for three different frequencies.

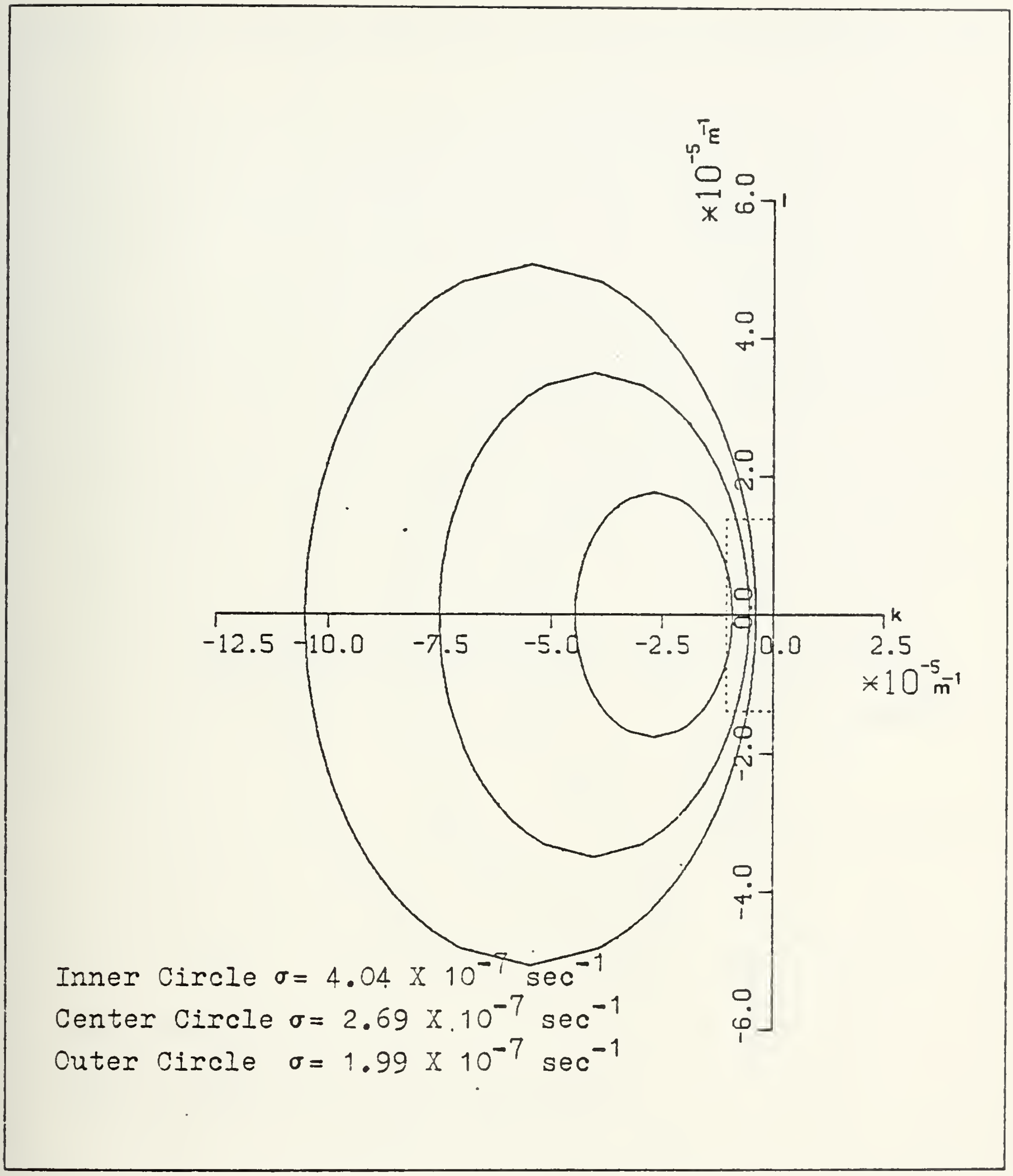

Figure 27. Locus of Wave Number Vectors for Mode 1 at 18.3N

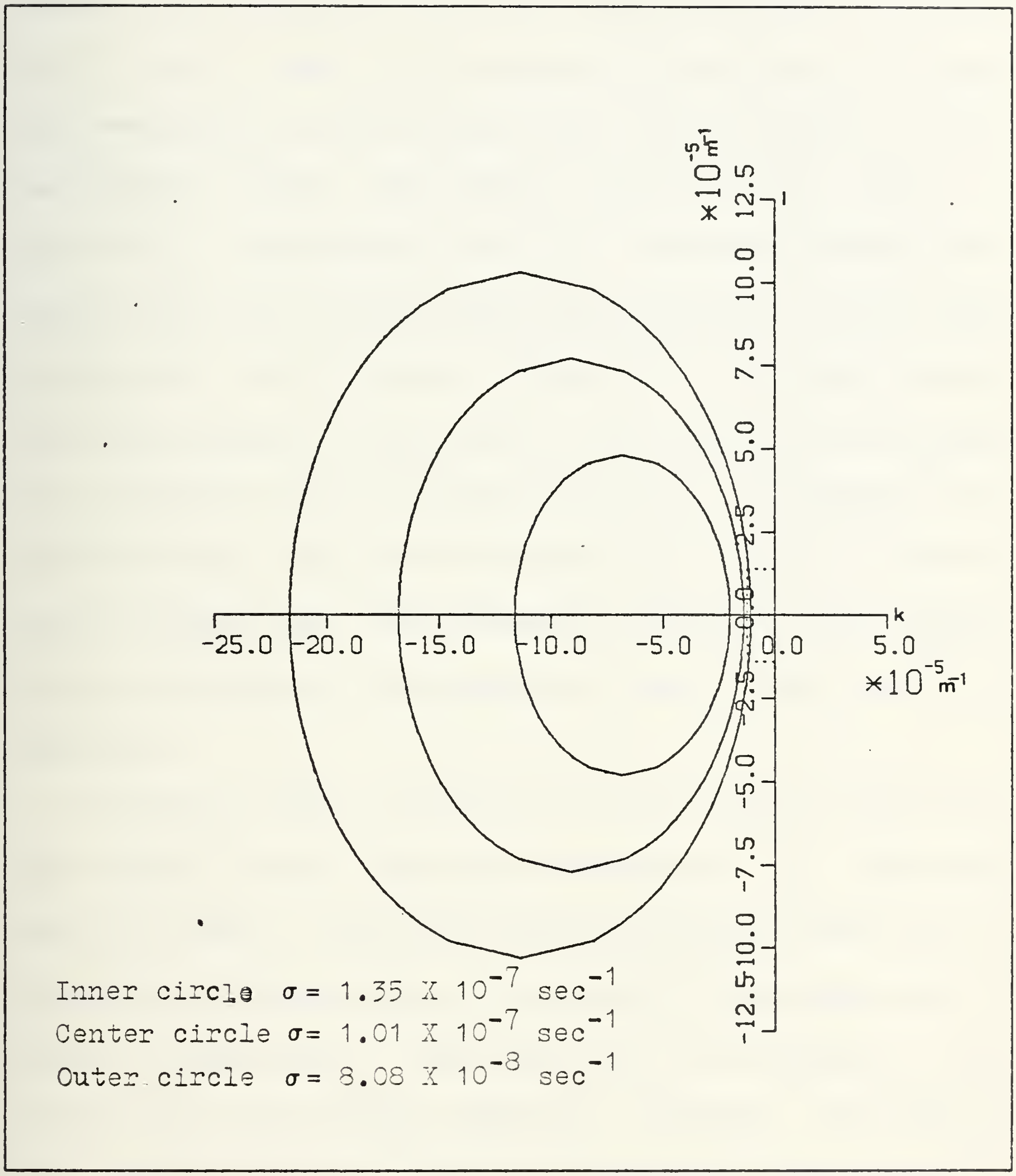

Figure 28. Locus of Wave Number Vectors for Mode 1 at 36.6N

The spacing between model grid points utilized in this study is on the order of 226 km in the north/south direction and 251 km (at 36N) in the east/west direction. The shortest wavelength resolvable by the model is equal to twice the spacing between grid points, which in this case is on the order of approximately 500 km. Therefore, Rossby waves resolvable by the model must have wavelengths greater than or equal to the 2Δd value, where Δd is the grid spacing. The wave numbers in the x and y direction which correspond to a wavelength which is greater than the 2Δd wavelength are located within the dotted rectangle in Figures 27 and 28. Stated another way, wave numbers outside of the boxed-in region correspond to wavelengths too small to be resolved by the model.

The inner circle in Figure 27 is the locus of wave numbers found when a frequency corresponding to a six-month period is used. The middle circle and outer circle are for frequencies corresponding to periods of nine months and 12 months, respectively. Note that due to the different scale of each axis the circles appear as ellipses. Portions of all three circles fall within the enclosed region indicating that wavelengths greater than the 2Δd wavelength can occur

at the aforementioned frequencies (periods). The circles in Figure 28 are for frequencies corresponding to periods of 18 months (inner circle), 24 months (middle circle) and 30 months (outer circle), respectively. It is noted that at 36.6N only waves having a period of about 30 months or greater have wavelengths long enough to be resolvable by the model. It follows that waves of $4\Delta d$ or $8\Delta d$ would have even greater periods. Therefore, increasing latitude requires an increase in the Rossby wave period to allow for wavelengths long enough to be resolved by the model grid spacing. Additionally, using equation (11), it may be shown that for wavelengths that are resolved by the model grid, $k^2 + \ell^2 \ll \lambda_n^2 f^2$ and thus the period $2\pi/\sigma$ must be larger than the cutoff period. At high latitudes such long periods would not be well resolved by the ten-year simulation. Thus, even though low deviations result at high latitudes (column 5 of Table II) the isotherm displacement variability cannot be attributed to actual Rossby waves with any degree of certainty.

IV. CONCLUSIONS AND RECOMMENDATIONS

Based upon the preceeding analysis the following results are summarized:

- On the average, free baroclinic Rossby wave signature in the model simulated isotherm displacement fluctuations is evident in the time domain for the selected grid points south of 40N.
- At the selected grid points south of 40N the first baroclinic mode shows predominance.
- Based upon the locus of wave number ellipses, Rossby waves at the appropriate periods are long enough to be resolvable within the model grid spacing.
- Based upon the deviation term, certain times within the ten-year model run period indicate that the first five baroclinic modes do not adequately fit the isotherm displacement fluctuations (i.e., the deviation is high, therefore, the isotherm displacement fluctuations cannot be fully explained by baroclinic free Rossby waves).
- At selected grid points north of 40N the analysis results are inconclusive.
- There is reasonably good agreement between the analysis results at model grid point 30.5N 139.1W and that conducted by Emery and Magaard (1976) for weather station November (30N 140W).

The results stated in point number five above, are a product of several factors. The model run time (ten years) sets a constraint upon the periods that may be adequately resolved by the analysis method. The cutoff periods of the selected grid points north of 40N gradually begin to approach a five-year period, and wavelengths resolved by the model grid

result in periods considerably greater than the cutoff (minimum) period. Periods greater than five years can not be adequately resolved by the analysis method. A longer run time is required. Secondly, since the ocean model is a "fresh" water model the effect is to dimenish the magnitude of the Brunt—Väisälä frequency, particularly at higher latitudes. This results in eigenvalues that are large compared to "real" ocean values (λ is inversely proportional to N). The larger eigenvalues then, in turn, increase the value of the cutoff period more than what occur when only the Coriolis parameter is considered. Finally, a seasonal signal, resulting from the seasonally varying model input parameters, dominates the isotherm displacement fluctuations over a greater portion of the water column at the northern selected grid points. Thus, the seasonal signal, which is primarily a thermodynamic effect, contaminates the first five modes.

Based upon these results several recommendations for further research may be set forth:

- The seasonal signal resulting from thermodynamic effects should be removed. This could be achieved by either neglecting the model layers above the main thermocline or by applying a filter technique to remove the the regular seasonal signal. The former suggestion would be impractical at the high latitude model grid points, however, due to the penetration of the seasonal signal down to the bottom of the water column.

- This study set the mean current equal to zero. Further studies should include the mean current in the analysis, particularly in the region of the California current, and North Pacific Current. A study by Kang and Magaard (1979) has shown that the North Pacific Current has a significant impact on the first baroclinic shear mode.

- Since the model neglects salinity further research should study the feasability of incorporating salinity. This would provide for more realistic density profiles and improve the analysis results at the higher latitudes.

- The mechanisms which produce Rossby waves in the North Pacific Ocean is still not fully understood. The analysis has shown that certain time periods within the model run period south of latitude 40N cannot be explained fully by the first five baroclinic modes. Apparently some other factor is involved. Further research could be done to isolate any peculiarities in the the synoptic wind field used as model input since the six-hourly synoptic wind was the only varying parameter from one year to the next. The study should also be extended to investigate the source of Rossby waves (i.e., whether they result from large-amplitude variations of the wind stress curl near the eastern boundary as hypothesized by White and Saur (1981) or whether some other mechanism is involved).

- All further studies should include comparison to appropriate observational studies when available, and thereby include a model evaluation.

This study has been a first step in analyzing the low frequency dynamics of the Haney (1980) ocean model below the mixed layer. A complete understanding of the dynamics of the large-scale variability of the ocean temperature field below the mixed layer (thermocline) is the primary goal. This understanding will in turn lead to improvements in the ocean model and its diagnostic and prognostic capabilities, the ultimate goal.

LIST OF REFERENCES

Adamec, D., R.L. Elsberry, R.W. Garwood, Jr. and R.L. Haney, 1981: An embedded mixed-layer-ocean circulation model. *Dynamics of Atmospheres and Oceans*, *6*, 69-96.

Emery, W.J., and L. Magaard, 1976: Baroclinic Rossby waves as inferred from temperature fluctuations in the eastern Pacific. *J. Mar. Res.*, *34*, 365-385.

Haney, R.L., 1980: A numerical case study of the development of large-scale thermal anomalies in the central North Pacific Ocean. *J. Phys. Oceanogr.*, *10*, 541-556.

Hildebrand, F.B., 1956: *Introduction to Numerical Analysis*. McGraw-Hill, 511 pp.

Kang, Y.Q., and L. Magaard, 1979: Stable and unstable Rossby waves in the North Pacific Current as inferred from the mean stratification. *Dynamics of Atmospheres and Oceans*, *3*, 1-14.

Kang, Y.Q., and L. Magaard, 1980: Annual baroclinic Rossby waves in the central North Pacific. *J. Phys. Oceanogr.*, *10*, 1159-1167.

Magaard, L., 1983: On the potential energy of baroclinic Rossby waves in the North Pacific. *J. Phys. Oceanogr.*, *13*, 38-42.

Pedlosky, J., 1979: *Geophysical Fluid Dynamics*. Springer-Verlag, 624 pp.

Preisendorfer, R.W., and F.I. Gonzalez, Jr., 1973: Classic Canal Theory. Hawaii Institute of Geophysics Rep. HIG-73-14, 284 pp.

Price, J.M., and L. Magaard, 1980: Rossby wave analysis of the baroclinic potential energy in the upper 500 meters of the North Pacific. *J. Mar. Res.*, *38*, 249-264.

Willmott, A.J., and L.A. Mysak, 1980: Atmospherically forced eddies in the northeast Pacific. *J. Phys. Oceanogr.*, *10*, 1769-1791.

White, W.B., and J.F.T. Saur, 1981: A source of annual baroclinic waves in the eastern subtropical North Pacific. *J. Phys. Oceanogr.*, *11*, 1452-1462.

INITIAL DISTRIBUTION LIST

		No. Copies
1.	Defense Technical Information Center Cameron Station Alexandria, VA 22314	2
2.	Library, Code 0142 Naval Postgraduate School Monterey, CA 93940	2
3.	Professor Robert J. Renard, Code 63Rd Department of Meteorology Naval Postgraduate School Monterey, CA 93940	1
4.	Professor Christopher N. K. Mooers, Code 68Mr Department of Oceanography Naval Postgraduate School Monterey, CA 93940	1
5.	Professor Robert L. Haney, Code 63Hy Department of Meteorology Naval Postgraduate School Monterey, CA 93940	1
6.	Professor Andrew J. Willmott, Code 68Wt Department of Oceanography Naval Postgraduate School Monterey, CA 93940	1
7.	Professor Lorenz Magaard Department of Oceanography University of Hawaii Honolulu, HI 96822	1
8.	Professor Rudolf W. Preisendorfer, Code 63Pw Department of Meteorology Naval Postgraduate School Monterey, CA 93940	1
9.	Lt. Arno H Rutsch 856 Oakridge Drive St. Joseph, MI 49085	2
10.	Director Naval Oceanography Division Naval Observatory 34th and Massachusetts Avenue NW Washington, D.C. 20390	1

11. Commander 1
Naval Oceanography Command Central
NSTL Station
Bay St. Louis, MS 39522

12. Commanding Officer 1
Naval Oceanographic Office
NSTL Station
Bay St. Louis, MS 39522

13. Commanding Officer 1
Fleet Numerical Oceanography Center
Monterey, CA 93940

14. Commanding Officer 1
Naval Ocean Research and Development
Activity
NSTL Station
Bay St. Louis, MS 39522

15. Commanding Officer 1
Naval Environmental Prediction Research
Facility
Monterey, CA 93940

16. Chairman, Oceanography Department 1
U.S. Naval Academy
Annapolis, MD 21402

17. Chief of Naval Research 1
800 N. Quincy Street
Arlington, VA 22217

18. Office of Naval Research (Code 422PO) 1
Naval Ocean Research and Development
Activity
NSTL Station
Bay St. Louis, MS 39522

19. Commander 1
Oceanographic Systems Pacific
Box 1390
Pearl Harbor, HI 96860

20. Library Acquisitions 1
NCAR
P.O. Box 3000
Boulder, CO 80307

Thesis
R9295
c.1

201741

Rutsch

Baroclinic Rossby
wave signature in a
general circulation
ocean model.

19 MAR 84 10569 ~~12856~~

201741

Thesis
R9295
c.1

Rutsch

Baroclinic Rossby
wave signature in a
general circulation
ocean model.

thesR9295
Baroclinic Rossby wave signature in a ge
3 2768 001 97022 1
DUDLEY KNOX LIBRARY